231

THE PHOTOCHEMISTRY OF RHODIUM(III) AMINE COMPLEXES

by

Frank Peter Jakse

B.S., Illinois Benedictine College, 1975

A MASTER'S THESIS

submitted in partial fulfillment of the

requirements for the degree

MASTER OF SCIENCE

Department of Chemistry

KANSAS STATE UNIVERSITY
Manhattan, Kansas

1978

Approved by:

John Ritter

Major Professor

To Elizabeth

ACKNOWLEDGEMENT

I would like to thank Dr. John D. Petersen for his assistance and encouragement. His knowledge of the subject and enthusiasm for the research have been invaluable for the completion of this work and are truly appreciated.

Gratitude is expressed to Dr. Keith F. Purcell for the many hours of helpful consultation and discussion.

Finally, I wish to acknowledge Dr. Petersen's research group, Joe, Dave, Janette, and Kurt, for their friendship and help in maintaining a proper perspective of life.

TABLE OF CONTENTS

TABLE OF CONTENTS (continued)

LIST OF TABLES

LIST OF FIGURES

INTRODUCTION

Photochemistry

In general, a photochemical reaction can be thought of in terms of a bimolecular process involving reactant A and a photon of energy, $h\nu$, to produce a Franck-Condon electronic excited state, B* (reaction 1).

$$A + h\nu \longrightarrow B^* \quad \text{excitation} \tag{1}$$

B* then dissipates energy either by radiative or nonradiative deactivation back to the ground state A, or by undergoing a chemical reaction to form C (reactions 2-4).

$$B^* \xrightarrow{k_r} A + h\nu \quad \text{radiative deactivation} \tag{2}$$

$$B^* \xrightarrow{k_n} A + \Delta \quad \text{nonradiative (thermal) deactivation} \tag{3}$$

$$B^* \xrightarrow{k_p} C \quad \text{product formation} \tag{4}$$

The quantum yiel (or efficiency, Φ, for the photochemical reaction (equation 4), can be expressed in terms of the rate constants in equation 4, using a steady-state approximation for excited state B*; i.e. $\frac{d[B^*]}{dt} = 0$.

$$\Phi_C = \frac{k_p}{k_r + k_n + k_p} \; ; \; \Phi_{lum.} = \frac{k_r}{k_r + k_n + k_p}$$

If B* is not the excited state directly populated by excitation, then the term, Φ_{IC}, representing the efficiency of internal conversion from the initially populated state(s) to the reactive state, B*,

must be included in the quantum yield calculation. Also, τ, the measured lifetime of the emitting excited state, is equal to the reciprocal of the sum of all rate constants that represent processes which deactivate the excited state. Therefore, inclusion and substitution of these terms

$$\tau_m = \frac{1}{\Sigma_i k_i} = \frac{1}{k_r + k_n + k_p} \tag{5}$$

in our quantum yield equation results in

$$\Phi_c = \Phi_{IC} \times k_p \times \tau_m \tag{6}$$

A Jablonski diagram (Fig. 1) schematically demonstrates the various reaction and energy dissipation processes described above. A* represents the initially populated excited state(s) mentioned above. Therefore,

$$\Phi_{IC} = \frac{k_1}{k_1 + k_2 + k_3} \tag{7}$$

and:

$$\Phi_C = \frac{k_1}{k_1 + k_2 + k_3} k_p \cdot \tau_m \tag{8}$$

Assume A and A* are states of identical spin multiplicity, S, whereas B* is of a different spin multiplicity, R. Rate constant, k_2, represents a fluorescence radiative deactivation ($^SA^* \xrightarrow{k_2} {}^SA + h\nu'$) and

FIGURE 1 : Jablonski Diagram Illustrating Electronic Excitation ($A^* \longleftarrow A$) and Excited State Processes.

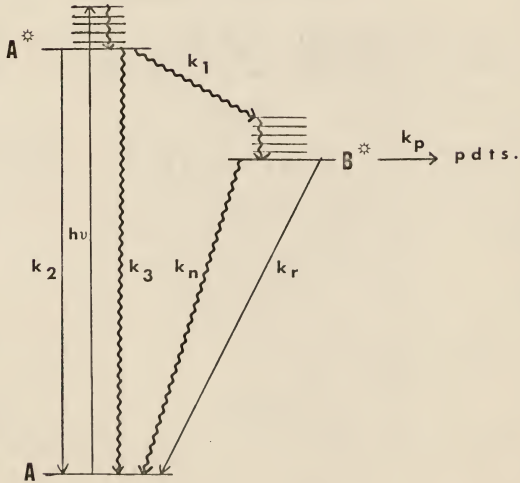

rate constant k_r, signifies a phosphorescence radiative deactivation ($^rB^* \xrightarrow{kr} {}^sA + h\nu''$); where $h\nu'$ and $h\nu''$ are fluorescent and phosphorescent emission photons, respectively. Phosphorescence lifetimes ($\sim 10^{-7}$ sec.) are usually longer than fluorescence lifetimes (10^{-13} sec.) because the former process involves a spin-forbidden process, and the rate constant for phosphorescence is dependent on spin-orbit coupling.[1]

Excited States:

The three types of excited states observed for transition metal complexes are: 1) ligand field (LF); 2) internal ligand (IL); 3) charge transfer (CT). The charge transfer type of excited state can be further classified into three categories:

a) charge transfer to metal (CTTM); $M^{+n}L \xrightarrow{h\nu} M^{(n-1)+}L^{+}$. An electron located in a molecular orbital, mainly ligand in character, is transferred to an m.o. mainly metal in character. If the metal center, $M^{(n-1)+}$, is substitution labile, a redox reaction takes place yielding solvated $M^{(n-1)+}$ and L^{+} ions. Due to the large transfer of charge accompanying CTTM excitation, a large solvent effect is observed for this excited state chemistry.[1]

b) Charge transfer to ligand (CTTL); $M^{+n}L \xrightarrow{h\nu} M^{(n+1)+}L^{-}$. An electron located in a molecular orbital, mainly metal in character, is transferred to an m.o. mainly ligand in character. Similar to CTTM, CTTL excitation may result in ligand substitution, dependent on the substitution liability of the $M^{(n+1)+}$ center. In the CTTL state, however, the metal center undergoes pseudo-oxidation, whereas, in the CTTM state, pseudo-reduction of the metal center occurs.

c) Charge transfer to solvent (CTTS); $M^{+n}L \xrightarrow{h\nu} M^{(n+1)+}L + e^{-}_{solv.}$. Very little is known about CTTS excited states in transition metal ions because their UV absorption bands are usually obscurred by other transition bands of greater intensity.[2]

Internal ligand (IL) excited states are located in the UV and evolve from $\pi \rightarrow \pi^*$ electronic transitions within a ligand. The oxidation state of the metal remains unchanged, but cleavage of intraligand bonds often occurs.[3] Often, the metal center represents only a minor perturbation on the ligand and the ligand photochemistry is similar whether it is free or coordinated.

Ligand field excited states (LF) result from d-d electronic transitions and are the excited states pertinent to this study. Considering a molecule of octahedral symmetry, the five metal d orbitals are no longer degenerate as in the free ion state, but are split into a triply degenerate set (d_{xy}, d_{xz}, d_{yz}) of t_{2g} symmetry and a higher energy doubly degenerate set (d_{z^2}, $d_{x^2-y^2}$) of e_g symmetry. (Fig. 2) In a Rh(III), d^6 low spin system of O_h symmetry (Fig. 3), a d-d transition represents an electron promoted from a nonbonding or π^* orbital (t_{2g}) to a σ^* orbital (e_g).[4] This transition produces an angular and radial redistribution of charge, whereby electron density is increased in the area of the metal-ligand bond, and electron density in the area between the metal-ligand bonds is decreased. This effect favors ligand labilization. Utilizing a molecular orbital approach, ligand field excitation increases σ-antibonding character in the metal ligand bonds. Both approaches suggest why LF excitations, in general, lead to ligand labilization, and LF excited states seldom lead to redox

FIGURE 2 : Schematic Representation of the Five Metal d Orbitals. In an Octahedral Environment, the Orbitals are Split Into an e_g (d_z^2, $d_{x^2-y^2}$) Symmetry Set and a t_{2g} (d_{xy}, d_{xz}, and d_{yz}) Symmetry Set.

d_{z^2}

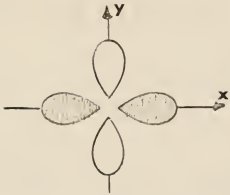

$d_{x^2-y^2}$

d_{xy}

d_{xz}

d_{yz}

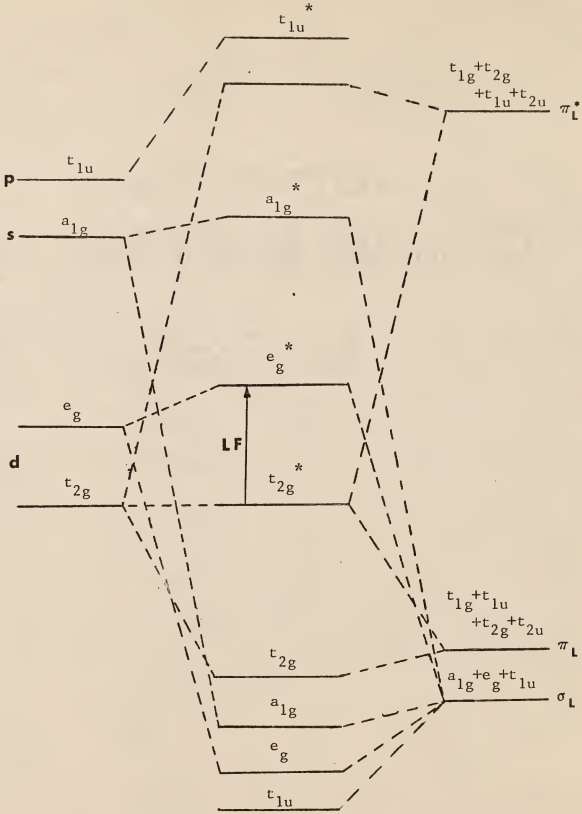

FIGURE 3 : Ligand Field Transition (LF) For Low Spin d^6 Metal Ion Complex of Octahedral Symmetry.

reactions involving the central metal atom. Ligand field excited state reactivity for complexes of lower symmetry will be treated further in the photochemistry discussion of this paper. Since no radial redistribution of charge occurs to the extent found in CT excited states, LF energies are little affected by solvent polarity changes.

Ligand field excited state energies lie in the UV-visible region of the spectrum and are dependent upon the ligand environment and the central metal atom and oxidation state. The Spectrochemical Series is an arrangement of ligands and metals in order of increasing orbital splitting (Fig. 4).[5]

Ligands can alter the d-orbital energies through σ- and π- effects. A combination of a weak σ-donor and strong π-donor for a particular ligand produces a small orbital splitting, whereas a strong σ- and weak π-donor ligand results in a large orbital energy difference. The reverse correspondence between the ligand Spectrochemical Series and the general electronegativity series, (halogen) < (oxygen) < (nitrogen) < (carbon), illustrates the importance of σ-donating effects. Further arrangements in the Spectrochemical Series can be rationalized in terms of π effects within a particular group. For example, the higher position of H_2O than of OH^- ligand is probably due to the fact that OH^- has two pi donor pairs while H_2O has only one.[5]

These σ- and π-donor properties of the ligands on a metal center can alter the relative energies of the molecular orbitals and, hence, change the energies of ligand field transitions in the complex's electronic spectrum of a complex.

FIGURE 4. THE SPECTROCHEMICAL SERIES.

LIGANDS: $I^- < Br^- < Cl^- < {}^*SCN^- < F^- \sim$ urea $< OH^- <$ ACETATE $<$ OXALATE $< H_2O <$ ${}^*NCS^- <$ GLYCINE $<$ PYRIDINE $\sim NH_3 <$ en $< SO_3^{*-2} <$ BIPYRIDINE $\sim$ o-PHEN $<$ ${}^*NO_2^- < CN^-$

(* Labels donor atom)

METALS: $(Mn^{+2} < Ni^{+2} < Cr^{+2} < Fe^{+2} < V^{+2}) < (Fe^{+3} < Cr^{+3} < V^{+3} < Co^{+3}) < Mn^{+4}$ $< (Mn^{+4} < (Mo^{+3} < Rh^{+3} < Ru^{+3}) < Pd^{+4} < Ir^{+3} < Re^{+4} < Pt^{+4}$

For the complexes $Rh(en)_2XY^{+n}$, whose photochemistry is studied in this research, spectral changes, observed in the difference spectrum of photolyzed sample *versus* "dark" sample (see Experimental section below), are indicative of changes in the inner coordination sphere produced by labilization of one ligand and coordination of another.

Since the low-spin d^6 metal systems (as well as d^3) have singly degenerate ground states, assignments of excited states can be deduced from the electronic spectra with relative ease, and the reaction observed upon irradiation can be accurately attributed to a specific excited state.

LF Reactivity of Cr(III) Amines

For photosubstitution reactions of the type shown in equation (9),

$$CrA_nB_{6-n} \xrightarrow{h\nu,\ S} CrA_{n-1}B_{6-n}S + A \qquad (9)$$

the solvated ligand A, can originate from n number of stereochemical sites in the primary coordination sphere. The stereochemistry of the photolysis product may seem independent of labilization site, but in order to formulate a general mechanism, applicable to all Cr(III) amine systems, the exact parentage of the photosolvated ligand must be determined.

For example, when $[Cr(NH_3)_5Cl]^{+2}$ is irradiated in the ligand field region (equation 10)[6], ammine aquation is the dominant photoreaction.

$$Cr(NH_3)_5Cl^{+2} \xrightarrow[H_2O]{h\nu} \underline{cis}\text{-}Cr(NH_3)_4(OH_2)Cl^{+2} + NH_3 \qquad (10)$$

$$\Phi_{NH_3} = 0.35\text{-}0.40$$

$$\Phi_{Cl} = 0.005\text{-}0.007$$

The photolabilization of ammine is consistently observed for other mono-substituted Cr(III) pentaamines;[7,8] however, these complexes all react thermally by losing the unique ligand.[9]

Reaction (10) may be thought of as occuring through two possible reaction paths:

1) A $\underline{cis}$-NH_3 ligand is photoaquated without rearrangement to yield directly the $\underline{cis}$-configuration of the photoproduct; or

2) The primary photochemical reaction involves labilization of the trans-NH_3 followed by subsequent thermal rearrangement to the cis product.

Further work with ^{15}N-labelled complexes[10] and with two ethylenediamine bidentate ligands ($H_2N-CH_2CH_2NH_2$) in place of four ammonias[11a,b] has shown that the initial photochemical process is predominant labilization of the trans-amine ligand with the appropriate thermal rearrangement to cis-product.

These results agree with a set of semiempirical rules, formulated by Adamson[12], for ligand field reactivity of mixed-ligand chromium(III) complexes:

1) Labilization occurs along the axis of the octahedron having the smallest average crystal field;

2) If the labilized axis contains two different ligands, the ligand of greater field strength is preferentially aquated.

Zink's molecular orbital approach[13a] accounts for the particular ligand labilized by the nature of the π^* orbital depopulation and increased σ^* orbital population.

While both Zink's molecular orbital treatment and Adamson's rules-based mechanism have been rather successful in predicting preferential ligand labilization upon LF excitation of mixed ligand Cr(III) amine complexes, neither approach accounts for the rearrangement that so frequently accompanies the photosubstitution of these species.

Table 1 lists the thermal and photochemical data for several Cr(III) complexes. One can see from the table that the "slow" thermal reaction will not interfere with the determination of photosubstitution efficiency

for the Cr(III) complexes listed. Similar behavior is observed in the d^6 systems of cobalt(III) and rhodium(III), as will be seen below.

TABLE I. Cr(III)AMINE THERMAL AND PHOTOCHEMICAL AQUATION DATA

COMPLEX	$\lambda_{irr.}$	PHOTOPDT.	Φ	$k_{THERMAL}$, sec^{-1}	REF.
$[Cr(NH_3)_6]^{+3}$	452	$[Cr(NH_3)_5(H_2O]^{+3}$	0.26	1×10^{-7}	48, 49
$[Cr(en)_3]^{+3}$	434	$[Cr(en)_2(enH)(H_2O)]^{+4}$	0.37	----	50
trans$[Cr(NH_3)_4Cl_2]^{+}$	540	cis$[Cr(NH_3)_4(H_2O)Cl]^{+2}$	0.44	----	51
trans $Cr(en)_2Cl_2^{+}$	540	$\geq$70% cis$[Cr(en)_2(H_2O)Cl]^{+2}$	0.32	2.2×10^{-5}	52, 49
$Cr(NH_3)_5Cl^{+2}$	546	cis isomer	$\Phi_{NH_3} = 0.36$ $\Phi_{Cl} = 0.005$	7.3×10^{-6}	53, 49
cis$[Cr(en)_2Cl_2]^{+}$	540	$[Cr(en)(enH)Cl_2(H_2O)]^{+2}$	0.13	33×10^{-5}	52, 49

LF Reactivity of Co(III) Amines

Table 2 lists a series of Cobalt(III) amine complexes and their pertinent thermal and photochemical data. The quantum yields for the Co(III) complexes are considerably lower than the Cr(III) analogs, when "pure" ligand field excited states are produced. Charge transfer excitation readily reduces Co(III) to Co(II) (in 3F HNO_3, $E° \simeq +1.8v$), a labile metal center. To minimize CT character in a ligand field excitation, one usually irradiates at a wavelength on the low energy side of the lowest energy (longest wavelength) ligand field band, L_1.

The increased quantum yields for all L_2 versus L_1 excitations are attributed to absorption into the tail of the charge transfer band and consequently, production of Co^{+2} and solvated ligands.

Mechanistically, Adamson's Rules have been applied to the Cobalt(III) amine systems with varying degrees of success.[14a,b 17] Trans-$[Co(en)_2Cl_2]^+$ undergoes photoaquation[14a] by loss of Cl^- to yield a 70:30 trans/cis isomeric mixture of $[Co(en)_2(OH_2)Cl]^{+2}$. Trans-$[Co(cyclam)Cl_2]^+$, when irradiated at 488 nm[14], produces 100% trans-$[Co(cyclam)(OH_2)Cl]^{+2}$. The photosubstitution quantum yields of trans-$[Co(en)_2Cl_2]^+$ versus trans-$[Co(cyclam)Cl_2]^+$ is approximately 3, while for the two Cr(III) analogs, the ratio is 1000. These ratios, along with the moderate degree of retention of configuration. may indicate that stereomobility is not an important requirement for Co(III) photoaquation, as it is for the Cr(III) systems. Both species undergo photoaquation of chloro ligand, as predicted by Adamson's rules, but the different quantum yields show the rules to be incomplete and the rearrangement phenomenon is not considered under the rules.

TABLE 2: Co(III)AMINE THERMAL AND PHOTOCHEMICAL AQUATION DATA

COMPLEX	$\lambda_{irr.}$	PHOTOPDT.	Φ	$k_{thermal}$, sec^{-1} (25 C)	REF.
$Co(NH_3)_6^{+3}$	488	$Co(NH_3)_5(H_2O)^{+3}$	3.1×10^{-4}	very small	14a
$Co(en)_3^{+3}$			$<< 10^{-5}$	----	54
trans-$Co(en)_2Cl_2^+$	488	$Co(en)_2(OH_2)Cl^{+2}$ (72% trans, 28% cis)	0.0011	35×10^{-6}	14a, 49
$Co(NH_3)_5Cl^{+2}$	488		$\Phi_{NH_3} = 0.005$ $\Phi_{Cl} = 0.00017$	1.7×10^{-6}	14a
cis-$Co(en)_2Cl_2^+$	488	$Co(en)_2(OH_2)Cl^{+2}$ (70% trans, 30% cis)	0.0024	24×10^{-6}	14b, 49

The ligand field photolysis of cis-$[Co(en)_2Cl_2]^+$ in acidic solution consists of chloride aquation to yield 70 - 75% trans-$[Co(en)_2(OH_2)Cl]^{+2}$ and 25 - 30% cis-$[Co(en)_2(OH_2)Cl]^{+2}$, after correction for secondary photochemical processes.[14b] Adamson's Rules can be successfully applied to this system, if an "edge displacement" occurs along the reaction coordinate:

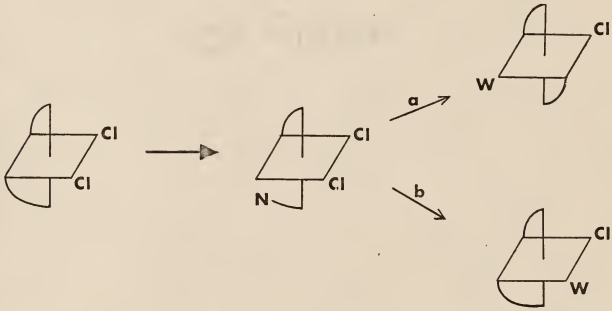

The rules predict preferential labilization of the strong field ligand (N on one end of ethylenediamine *) along the weak field axis (N-Co-Cl,---). Recoordination of the ethylenediamine (path a) by "edge displacement" of chloro ligand yields the trans-$[Co(en)_2(OH_2)Cl]^{+2}$ product.

This scheme does not explain the entire reaction, however. The minor yield of cis product may be due to recoordination at the position trans to the original coordination site or due to direct chloride aquation. The former explanation is highly improbable, while the latter

is in violation of the "rules". Also, if one end of ethylenediamine labilizes, protonation is likely to occur in the acidic solution (pH=2) to yield $[Co(en)(enH)(OH_2)Cl_2]^{+2}$ or $[Co(en)(enH)(OH_2)_2Cl]^{+3}$. Alexander and Spillart[15] have successfully prepared and isolated cis-$[Co(en)_2(enH)Cl]Cl_3$ by a thermal process, reducing the likelihood of ethylenediamine recoordination.

Analyses of the ligand field photochemistry of cis- and trans-$[Co(en)_2(NH_3)Cl]^{+2}$ demonstrate similar ambiguities when Adamson's Rules are used as a mechanistic approach.

Consider first the trans-$[Co(en)_2(NH_3)Cl]^{+2}$ species, where two bidentate ethylenediamine ligands replace four ammonias with negligible ligand field change. The ratio of quantum yields for ammonia aquation for t-$[Co(en)_2(NH_3)Cl]^{+2}$ versus $[Co(NH_3)_5Cl]^{+2}$ is approximately 1:5 (Table 2), but the important result is that the Φ_{NH_3}/Φ_{Cl} ratio is comparable in the two complexes. According to the rules, this is expected for predominant labilization of a nitrogen ligand trans to a chloride. If random labilization occurs for $[Co(NH_3)_5Cl]^{+2}$, the Φ_{NH_3}/Φ_{Cl} value of 3 would represent 0.6 efficiency for any of five ammonias relative to chloride loss. Hence, Φ_{NH_3}/Φ_{Cl} would be 0.6 for trans-$[Co(en)_2(NH_3)Cl]^{+2}$.

The much higher ratio certainly supports the rules-based mechanism for trans-$[Co(en)_2(NH_3)Cl]^{+2}$, however, photoaquation of chloride also occurs with a significant quantum yield, contrary to a strict application of Adamson's mechanism.

For the cis-$[Co(en)_2(NH_3)Cl]^{+2}$ complex, the rules predict labilization along the weakest field axis, preferential labilization of one end of

an ethylenediamine trans to chloride, as in reaction (2) of Figure 5[16]. Edge displacement of the ammine ligand produces the trans-$[Co(en)_2(OH_2)Cl]^{+2}$ product. Chloride photoaquation also occurs, however, to yield cis-$Co(en)_2(OH_2)(NH_3)^{+3}$ in a stereoretentive process (reaction 1). The quantum efficiencies for the two reactions are similar and Adamson's second rule, concerning preferred labilization of the stronger field ligand, breaks down. Also, the edge displacement by an open-ended ethylenediamine of reaction (2), along with reactions (3), (5) and (6) is doubtful. The product from reaction (4) is not observed in the photolyzed sample.

Hence, reactions (1) and (7) remain to account for the products formed. While, reaction (1) is a stereoretentive process, (consistent with the earlier contention that Co(III) amines demonstrate less stereomobility in their photochemistry than the Cr(III) analogs) reaction (7) entails extensive ligand rearrangement of a 5-coordinate intermediate in order to yield the trans-$Co(en)_2(OH_2)Cl^{+2}$ photoproduct.

Sheridan and Adamson[17] studied the LF photochemistry of several Co(III) mixed ligand amine complexes with increased chelation than the bis(ethylenediamine) species in order to readily test adherence to the rules and any stereochemical changes that might occur. The reactions (11)-(13) and principal products of several of the complexes are given below:

trans 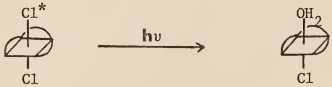

(11)

α cis 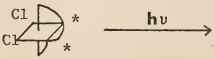

no reaction (12)

FIGURE 5 : Possible Reaction Scheme for LF Photolysis of <u>cis</u>-$Co(en)_2(A)Cl^{+2}$ ($A = NH_3$, $W = H_2O$). (*) Indicates Site of Labilization.

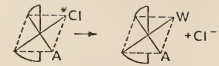
*Cl
A
W
+Cl⁻
A

(1)

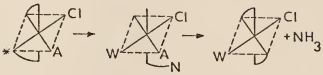
Cl
*
A
Cl
W
A
N
Cl
W
+NH3

(2)


Cl
A
*
Cl
N W
A
Cl
+NH3
W

(3)

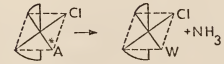
Cl
*
A
Cl
+NH3
W

(4)

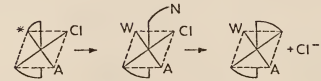
*
Cl
A
N
W
Cl
A
W
+Cl⁻
A

(5)

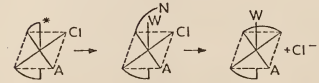
*
Cl
A
N
W
Cl
A
W
+Cl⁻
A

(6)

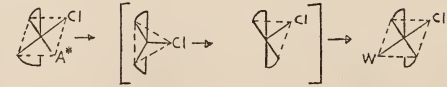
Cl
A*
Cl
Cl
W
Cl
+ NH3

(7)

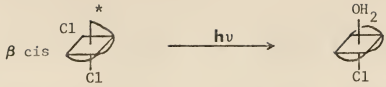

(13)

The trans-$[Co(trien)Cl_2]^+$ species undergoes photoaquation of Cl^- ligand in a stereoretentive process to yield trans-$[Co(trien)(OH_2)Cl]^{+2}$ (reaction 11), in agreement with Adamson's rules.

The two cis isomers of $[Co(trien)Cl_2]^+$ differ in photochemical reactivity: the cis α isomer undergoes no ligand photosubstitution (reaction 12), whereas the cis β isomer yields the trans-$[Co(trien)(OH_2)Cl]^{+2}$ complex (reaction 13). These preliminary results might be explained by application of Adamson's Rules: In the cis α isomer, the two secondary nitrogens (*) are the predicted sites of labilization, but chelation forces recoordination; in the cis β isomer, a primary nitrogen (*) is now labilized, and edge displacement of the chloro ligand cis to the labilized site followed by aquation yields the trans-$[Co(trien)(OH_2)Cl]^{+2}$.

These results could also be explained by labilization of chloride ligand, followed by rearrangement.

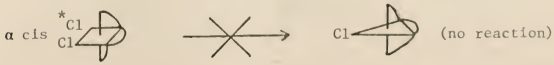

The cis α isomer is photochemically inert because of its inability to form a five-coordinate intermediate of trigonal bipyramid geometry[18], due to the limited bite (90°) of the ethylenediamine.

The cis β isomer, however, is capable of labilizing either chloride, and rearranging to either a trigonal bipyramid or square pyramid in order to aquate in a stereospecific manner (reaction 15 and 16).

(15)

β cis

(16)

In support of a square pyramidal intermediate, Sheridan observed the following reaction:[19]

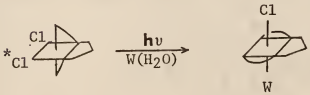

(17)

The three-carbon bridge is now capable of spanning the 120° angle between the equatorial nitrogens of the proposed trigonal-bipyramidal intermediate; however, trans coordination by H_2O is still blocked by the three carbon bridge. Collapse to a square pyramidal structure accounts for the

reactivity and stereospecificity of this particular reaction.

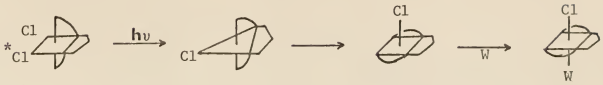

The reactions mentioned above clearly illustrate the limited applicability of Adamson's Rules to Co(III) amine systems. The Co(III) photochemistry lacks the stereospecificity found in the Cr(III) photochemistry. Rearrangement is less prevalent in the Co(III) systems versus Cr(III) (cf. cis and trans-$[Cr(en)_2Cl_2]^+$), and it might prove interesting to study another d^6 system, Rh(III), with special attention devoted to stereochemical processes.

Due to the various reaction products of the Co(III) amine photochemistry and lack of luminescence data, several reaction pathways have been proposed for the cobalt(III) metal systems[20,21], and caution should be exercised in comparing the two d^6 metal systems. Endicott and Ferraudi[21], have, in fact, proposed different reaction pathways for the photosubstitution reactions of Co(III) and Rh(III) acidopentaamine complexes. Their conclusions, based on approximate energies of the lowest triplet excited states, activation energies for thermal substitution processes, and magnitude and wavelength dependence of photosubstitution quantum yields are that Rh(III) complexes undergo excited state substitution reactions while the Co(III) ammine complexes aquate ligands via high energy state vibrational levels.

Some anomolous behavior between the two systems can be seen in the next section on Rh(III) ammines.

LF Reactivity of Rh(III) Amines

Throughout the discussions of both Cr(III) and Co(III) amine LF photosubstitution reaction, stereospecific labilization has been stressed in order to substantiate or confirm existing theories and/or semi-empirical rules regarding photochemical mechanisms.

In review, mixed ligand Cr(III) complexes of the type, $[CrA_4XY]^{+n}$, where A_4 = $4NH_3$, 2en, X=Cl, NH_3, and Y=Cl, OH_2, NH_3 undergo efficient photoaquation out of the lowest energy quartet excited state. Stereomobility occurs quite frequently in Cr(III) LF reactivity, and the photochemistry is generally different than the analogous thermal reactions.

The Co(III) photochemical reactions are different than the thermal reactions, but the photo-induced reactions lack the efficiency and high stereospecificity found in the Cr(III) amines.

The Co(III) amine photochemistry is not as well understood as the Cr(III) system for lack of luminescence data. Also, since cobalt(III) is easily reduced to Co(II) in solution, charge transfer reactions often complicate LF excited state studies. In lieu of these difficulties for cobalt(III) systems, a better, albeit more expensive, d^6 system is rhodium(III). The rhodium(III) amine systems have a well-characterized excited state reactivity based on extensive luminescence and photosubstitution data. Rh^{+3} is not easily reduced to Rh^{+2} and, therefore, photolysis in a CTTM band of a Rh(III) amine usually leads to substitution (Eq. 20) and not reduced products as in the Co(III) amines.

$$[Rh(NH_3)_5Cl]^{+2} + H_2O \xrightarrow[\Phi_{Cl} = 0.11]{h\nu(254nm)} [Rh(NH_3)_5(OH_2)]^{+3} \qquad (20)$$

Finally, the Rh(III) systems of interest (RhA_6^{+3}, RhA_5X^{+n}, cis- and trans-$[RhA_4X_2]^{+1}$, cis- and trans-$[RhA_4XY]^{+n}$ where A = NH_3, en/2, X = Cl, OH_2, Y = NH_3) have large quantum yields for photosubstitution reactions, yet, thermally, these complexes are relatively stable. A review of rhodium(III) ammine (eq. $Rh(NH_3)_6^{+3}$) LF photochemistry is necessary for 3 basic reasons:

1) The excited state reactivities have been well studied and characterized;

2) LF excitation leads to efficient labilization and solvation;

3) The disparate behavior of Cr(III) and Co(III) systems prevents us from predicting stereospecific mechanisms for Rh(III) LF excited state reactions. Thus, the unique Rh(III) ammine reactivity is the basis for the topic of this research, the stereochemical mechanism of Rh(III) amine LF excited state reactions.

Table 3 lists thermal and photochemical data for a series of Rh(III) ammine complexes. Thermal reactivity is low and does not complicate any of the photoreactions.

$[Rh(NH_3)_5Cl]^{+2}$ loses Cl^- to form $[Rh(NH_3)_5(OH_2)]^{+3}$ when irradiated at both 254 nm ($^1T_2 \leftarrow {}^1A_1$) and 350 ($^1T_1 \leftarrow {}^1A_1$). The Φ_{Cl} for both excitations are similar and suggests efficient intersystem crossing to a common substitution-reactive excited state.[22] This excited state is assigned as the lowest energy triplet state, based on the low temperature phosphorescence of $Rh(NH_3)_5Cl^{+2}$ and sensitization studies.[22] $[Rh(NH_3)_5Cl]^{+2}$ quenches the biacetyl phosphorescence and results in the same products as produced in the direct excitation, and with similar efficiency ($\Phi_{sens.}$ = 0.16).

TABLE 3: Rh(III)AMINE THERMAL AND PHOTOCHEMICAL AQUATION DATA

COMPLEX	$\lambda_{irr.}$	PHOTOPDT.	Φ	$k_{THERMAL}$, sec^{-1} (80°C)	REF.
$[Rh(NH_3)_6]^{+3}$	313	$[Rh(NH_3)_5(H_2O)]^{+3}$	0.075	----	23
trans$[Rh(NH_3)_4Cl_2]^{+}$	407	trans$[Rh(NH_3)_4(OH_2)Cl]^{+2}$	0.13	12.1×10^{-5}	36, 49
trans$[Rh(en)_2Cl_2]^{+}$	407	trans$[Rh(en)_2(OH_2)Cl]^{+2}$	0.047	10.4×10^{-5}	36, 49
$[Rh(NH_3)_5Cl]^{+2}$	380	$[Rh(NH_3)_5(OH_2)]^{+3}$	0.14	6.2×10^{-5}	22, 49
cis$[Rh(NH_3)_4Cl_2]^{+}$	365	trans$[Rh(NH_3)_4(OH_2)Cl]^{+2}$	0.33	----	27
cis$[Rh(en)_2Cl_2]^{+}$	350	trans$[Rh(en)_2(OH_2)Cl]^{+2}$ and other pdts.	0.056		28, 49

The data clearly indicates that the efficiency of intersystem crossing from singlet LF states populated by direct excitation to the reactive triplet states is unity ($\Phi_{isc} = 1.0$)(Fig. 6). Studies on other Rh(III) ammine systems[23,24,25,26] suggest a similarly high efficiency of conversion to the reactive lowest energy triplet state.

Ligand field irradiation of both cis[27] and trans-$[Rh(NH_3)_4Cl_2]^+$ [28] result in exclusive Cl^- labilization to yield trans-$[Rh(NH_3)_4(OH_2)Cl]^{+2}$ (Table 3). Ammine labilization is not observed in either photoreaction and, unless a cis → trans isomerization reaction preceeds labilization, the cis-$[Cl_2]^+$ species does not obey Adamson's Rules. Likewise, the chloropentaaminerhodium(III) species discussed above, reacts contrary to the rules when irradiated in its ligand field bands.

Petersen and Ford[23,29] observed the following LF excited state reactions:

$$[Rh(NH_3)_6]^{+3} \xrightarrow[H_2O]{h\nu} [Rh(NH_3)_5(OH_2)]^{+3} + NH_3 \qquad (21)$$

$$[Rh(NH_3)_5(OH_2)]^{+3} \xrightarrow[Cl^-]{h\nu} [Rh(NH_3)_5Cl]^{+2} + H_2O \qquad (22)$$

The photochemistry of the aquopentaamine rhodium(III) species is yet another example of Rh(III) photosubstitution contrary to Adamson's Rules, which predicts trans-NH_3 loss.

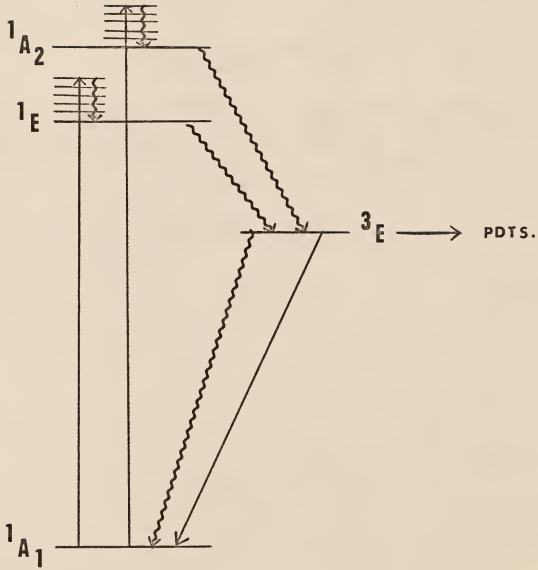

FIGURE 6 : Proposed Excited State Reactivity For $Rh(A)_5X^{+2}$ System.[22]

Statement of Problem

From this brief review of Co(III) and Rh(III) ammine LF photochemistry, it is obvious that Adamson's Rules are not successful in predicting the LF photochemistry of d^6 metal center systems. Also, such an interpretation does not account for the rearrangement or stereoretention phenomena that occur for certain complexes.

The purpose of this research is to formulate a general mechanism that accounts for: 1) the ligand field photosubstitution reactions of Rh(III) amine complexes; and, 2) the stereospecific nature of the photoreactions.

The LF photochemistry investigated involves the complexes, $Rh(en)_3^{+3}$, cis- and trans-$Rh(en)_2Cl_2^+$, and cis- and trans-$Rh(en)_2(NH_3)Cl^{+2}$. These chelated species are spectroscopically similar to the analgous Rh(III) ammine complexes, (whose photochemistry was discussed above), and, hence, the ligand photosubstitution of the chelated amine family can often be anticipated prior to experimentation. The efficiency of photosubstitution may vary, however, depending upon differences in radiative and/or nonradiative processes from the respective ligand field excited states. Also, the chelation of the nitrogen-base ligands will aid in elucidating the stereochemical changes that may occur in the course of the photochemical reaction.

EXPERIMENTAL

Chemicals

All chemicals and solvents were reagent grade and were used without further treatment or purification. Distilled water was redistilled from alkaline permanganate in an all-glass apparatus prior to use in synthetic and photochemical studies.

The en·2HCl salt was prepared by slowly adding through a condensor, 12 F HCl (analytical reagent grade) to anhydrous ethylenediamine (Fisher Scientific Company, certified) (2:1, v/v) in a round-bottom flask. A magnetic stir bar maintained homogeneity. The voluminous needle-like white crystals that formed were filtered on a large sintered-glass funnel under vacuum for several hours. (It took several days for the crystals to dry completely.)

Synthesis of Rh(III) Complexes

$[Rh(en)_3]Cl_3 \cdot 3H_2O$ - The tris(ethylenediamine)rhodium(III) chloride salt was prepared by the standard literature procedure.[30]

cis- and trans-$[Rh(en)_2Cl_2]NO_3$ - The nitrate salts of the two dichlorobis(ethylenediamine)rhodium(III) complexes were prepared as previously described,[31] with one minor modification. Small amounts of aqueous KOH were added to the refluxing solution every 30 seconds as opposed to 1-2 minute intervals, stated in the literature.[32]

cis-$[Rh(en)_2Cl_2]ClO_4$ - Conversion of the nitrate salt of the cis-dichloro complex into the perchlorate salt was accomplished by stirring 0.15 grams of the nitrate salt in a minimum of hot water (approximately 1.5 ml.), and immediately filtering the solution into 5 ml. of methanol which had been saturated with sodium perchlorate. After cooling for one hour, the yellow crystals were collected, washed with 100% ethanol, then ether, and dried under vacuum. Initial recovery of the complex corresponded to 70% yield.

trans-$[Rh(en)_2(OH_2)Cl](ClO_4)_2$ - The literature procedure[33] with minor modifications was used to prepare trans-$Rh(en)_2Cl(OH_2)(ClO_4)_2$. A 0.42 g. (0.89 mmol) sample of trans-$[Rh(en)_2Cl_2]ClO_4$ was added to a solution of $AgClO_4$ (0.89 mmol) (prepared by dissolving 0.115 g. of Ag_2O (Ventron Alfa Products, 99%) in a minimum of $HClO_4$ and filtering) and diluted to 5 ml. The solution was gently refluxed for 2.5 hours in a 25 ml. round bottom flask, fitted with a water-cooled condensor. Stirring was maintained with a magnetic stir

bar throughout the course of the reflux. The mixture was cooled to room temperature and filtered to remove the white AgCl precipitate. The filtrate was rotary-evaporated over steam to a golden yellow oil with pale yellow crystals forming after the addition of ethanol. The collected crystals were washed with ethanol, then ether, and dried under vacuum. A second crop of crystals was obtained by rotary-evaporation of the final filtrate. The total yield is 70.5%.

cis-$[Rh(en)_2(OH_2)Cl]^{+2}$ - The cis-$[(OH_2)Cl]^{+2}$ complex was prepared by a similar procedure, using 0.25 mmoles of cis-$[Rh(en)_2Cl_2]ClO_4$ and refluxing for 2.0 hrs. The complex was never isolated as the perchlorate salt, however, due to the small amount of product synthesized and its extreme solubility in aqueous media.

cis-$[Rh(en)_2(enH)Cl]Cl_3 \cdot 2H_2O$ - 0.5 g. (1.1 mmol) of $[Rh(en)_3]Cl_3 \cdot 3H_2O$ was dissolved in 35 ml deoxygenated 1F HCl. The solution was placed into a quartz tube and irradiated at 5°C for 4 days with three low pressure mercury lamps (Ultraviolet Industries, PCQ-X1). The solution was cooled with a fan and stirred with a magnetic stir bar throughout the photolysis.

The photolysis was considered complete when the absorption band at 301 nm ($Rh(en)_3^{+3}$) had reached a minimum with respect to the 345 nm band of the photoproduct. The solvent was removed from the system by rotary evaporation leaving a solid which was predominantly photoproduct with a small amount of starting material. If irradiation is continued for longer periods of time to try to minimize the amount of unreacted starting material, $[Rh(en)_3]^{+3}$,

a loss in absorbance at 345 nm and an increase at 406 nm results. Isolation of reasonably pure cis-$[Rh(en)_2(enH)Cl]Cl_3 \cdot 2H_2O$ was accomplished by minimizing the secondary processes and recrystallizing from 1 F HCl (photoproduct more soluble in 1 F HCl than $[Rh(en)_3]^{+3}$.

Anal. calcd. for $C_6H_{25}N_6Cl_4Rh \cdot 2\ H_2O$: C, 15.6%; H, 6.3%; N, 18.2%; Cl, 30.7% Found C, 15.6%; H, 6.4%; N, 18.4%; Cl, 32.8%

cis- and trans-$[Rh(en)_2(NH_3)Cl](NO_3)_2$ - The nitrate salts for both the cis and trans- isomers were prepared according to the published procedure,[31] with a minor adaptation. If an oil formed in the crystallization process,[31] (rather than the nitrate salt) the oil in the bottom of the beaker was isolated by decanting off most of the solvent. While kneading the oil with a rubber policeman, 10-15 ml. of solvent were slowly returned back into the beaker. Yield enhancements over literature values have been accomplished by this technique for both isomers. (cis: 71% vs lit. 40%, trans: 59% vs lit 4[illegible]%[31])

Trans-$[Rh(en)_2(NH_3)(OH_2)](NO_3)_3$ - A 10 ml. aqueous solution containing 0.338 mmoles trans-$[Rh(en)_2(NH_3)Cl](NO_3)_2$ and an equivalent amount of $AgNO_3$ was reflexed for 4.5 hours. The pale yellow solution was first cooled to room temperature, and, after filtering off the white AgCl salt, rotary-evaporated over low heat to dryness. The residue was dissolved in 1.5 ml. H_2O and the solution was filtered into 1.5 ml. cold concentrated HNO_3. 25 ml. of 100% ethanol was added to the solution and the cloudy white mixture was refrigerated for one hour. The white precipitate was collected on a sintered-glass funnel, washed with separate portions of ethanol

and ether, and dried under vacuum. Molar yield=59%.

Cis-$Rh(en)_2(NH_3)(OH_2)^{+3}$ was prepared similarly to the *trans* isomer from the *cis*$[(NH_3)Cl]^{+2}$ species, but the nitrate salt of the product was never isolated, due to the small amounts extreme solubility of the sample.

In cases where the product salt could not be isolated, all spectroscopic data was obtained *in situ*.

Apparatus

1) UV - Vis Spectra - All electronic spectra were obtained on a Cary Model 14 UV-vis spectrophotometer. Molar extinction coefficient values, for the compounds synthesized in this work, were measured using gravimetrically prepared samples. All spectra were obtained from 6 ml. samples contained in 2 cm. cylindrical supracil cells (Pyrocell Manufacturing Company, Inc.). Base lines corrections were run using pure solvent, excluding only the complex salt.

2) Magnetic Resonance Spectra - Proton-decoupled carbon-13 nmr spectra were obtained with a Varian XL-100-15 spectrometer operating at a frequency of 25.2 MHz and equipped with a Nicolet TT-100 Data System with quadrature phase detection and 20K of memory, allowing 16K data points, 8K points in the frequency domain for 3012 HA spectral width. All spectra were measured in D_2O (Sigma Chemical Company, approx. 99.8%)/H_2O (1:1, v/v) mixtures at concentrations varying between 0.05 and 0.3 M depending on the solubility and availability of the complex. One drop each of dioxane and 6 F HCl were added to each sample tube before obtaining a spectrum. The flip angle varied between 40 and 60° with a seven second delay between pulses. The number of pulses required to obtain a good signal-to-noise ratio was concentration dependent and varied from 512 to 14,816. The deuterium resonance of D_2O was used as the lock signal. Carbon-13 chemical shifts were measured relative to internal dioxane (Fisher Scientific Company, purified 1-4 dioxane) but are reported relative to external TMS. The conversion to external TMS was calculated with the relationship:

$$\delta \text{ ext. TMS} = \delta \text{ int. dioxane} + 67.40 \text{ ppm} \qquad (23)$$

Spectral reproducibility was > $\pm$ 0.03 ppm.

Techniques

All quantitative photolyses were performed at 25°C with an Oriel Universal Arc Lamp Source with a 200 W high pressure Hg short arc lamp. (See Fig. 7). The light beam first passed through an 8 cm. water cell (to remove IR components), a quartz collimating lens, and the appropriate interference filter (Oriel G-521-3130, G-522-3650, G-522-4047) before reaching the 6 ml. aqueous sample in cylindrical 2 cm. quartz window cell, supported in the light beam by a thermostated copper-jacket cell holder. Aqueous solutions of a particular complex were irradiated at a wavelength corresponding to the lowest ligand field band of the complex. During the course of all quantitative photolyses measurements, a similar 6 ml. sample from the same stock as the photolyzed sample was monitored for thermal reaction. This "dark" sample was used as a reference for monitoring absorbance changes of the photolyzed sample at a particular wavelength. Absorbance measurements were taken for: 1) a particular monitoring wavelength, selected for its large $\Delta\varepsilon$;

$$\Delta\varepsilon = \varepsilon_{pdt} - \varepsilon_{reactant} \tag{24}$$

2) the wavelength of irradiation at known time intervals of irradiation.

The quantum yield for product formation, Φ_{pdt}, was calculated by the following equation:

$$\Phi_{pdt} = \frac{\text{moles pdt formed}}{\text{einsteins absorbed}} = \frac{(\Delta A/\ell\cdot\Delta\varepsilon)V\cdot N_o}{I_{abs}\cdot t} \tag{25}$$

FIGURE 7 : Schematic Diagram of the Photochemical Apparatus.

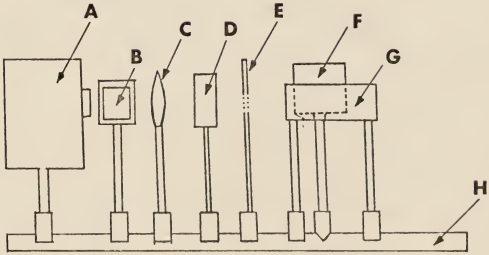

A LIGHT SOURCE

B IR FILTER

C COLLIMATING LENS

D WAVELENGTH SELECTOR FILTER

E LIGHT STOP

F MAGNETIC STIRRER

G THERMOSTATED CELL HOLDER

H OPTICAL BENCH

where ΔA is the difference in absorbance between reactant and product at the monitoring wavelength, l is cell pathlength in cm., $\Delta\varepsilon$ is the difference in molar absorptivity coefficient in terms of moles^{-1} cm^{-1}, V is the volume of the cell, N is Avogadro's number, 6.023×10^{23} quanta/einstein, I°_{abs} is the absorbed intensity in quanta/min., determined by ferrioxalate actinometry,[34] and t is the time of irradiation in minutes.

A computer analysis (Appendix 1) of the data for a series of reaction times yielded Φ_{pdt}, both incremental and overall (mean), and the per cent reaction for each time period (Appendix 1). A plot of Φ_{pdt}'s <u>versus</u> % reaction, extrapolated to 0% rxn. (when only reactant is absorbing light) yielded the initial quantum yield, Φ. Only initial quantum yields are reported in this work.

Ferrioxalate actinometry[34] was used to determine the incident intensity of light in quanta/minute. Actinometers were performed at the beginning and end of each photolysis experiment, and the mean of the two determinations was used in the computer analysis of the quantum yield.

A pH dependence study was done on the $[Rh(en)_3]^{+3}$ photochemistry Samples were adjusted to the desired pH with either HCl(pH 0-6) or NaOH (pH 8-12). NaCl was added to maintain the chloride concentration at 1 <u>M</u> for all aqueous solutions. For the photolyses of all other complexes in this study, aqueous 0.014 <u>N</u> $HClO_4$ was used as the solvent.

Photoproduct formation and proton consumption were compared for the LF photochemistry of $[Rh(en)_3]^{+3}$. Product formation quantum

yields were determined by the method mentioned above. A Beckman model #5 pH meter, equipped with an Orion Research Combination electrode (pH 91-02-00) was used for the pH measurements.

Infrared spectra were obtained for all complexes, isolated as salts, with a Perkin-Elmer 180 IR spectrometer. KBr pellets were prepared from 100 mg. oven-dried spectral grade KBr and 1-2 mg. of the complex salt.

RESULTS

Spectral Data

1) Infrared - The infrared data for the rhodium(III) complexes are given in Table 4. Several characteristic frequencies for these complexes are listed. The assignments were based on published results of analogous compounds.[31] Cis- and trans- isomers can be distinguished by observing a greater degree of splitting in the spectra of cis-isomers, particularly in the shape of the NH_2 asymmetric deformation frequency near 1600 cm^{-1} [31]. The spectra of trans-isomers generally contain a single peak while those of cis-isomers usually display a prominent shoulder above 1600 cm^{-1}.

The IR spectra of cis-$[Rh(en)_2(enH)Cl]^{+3}$ and $[Rh(en)_3]^{+3}$ differ slightly, with the former complex displaying broader peaks (especially around 3000 cm^{-1}) and an absorption at 300-350 cm^{-1} (Rh-Cl stretch).

2) C-13 nmr- The C-13 nmr data and assignments are given in Table 5 and Figure 8. The actual spectra are shown in Figures 9a - 9l. $[Rh(en)_3]^{+3}$ and all trans-$[Rh(en)_2XY]^{+n}$ species exhibited one resonance in their proton-decoupled C-13 spectra, whereas for all but two of the cis-$[Rh(en)_2XY]^{+n}$ species displayed four resonances: cis-$[Rh(en)_2Cl_2]^{+}$ and cis-$[Rh(en)_2(enH)Cl]^{+3}$ show two and six resonances, respectively, in their C-13 nmr spectra. The carbon atom chemical shift assignments will be reserved for the discussion section.

TABLE 4. INFRARED SPECTRAL DATA FOR Rh(III)COMPLEXES. FREQ. IN cm^{-1}.

COMPLEX	NH_2 ASYM DEFORM	CH_2 ROCK	Rh-N STRETCH
trans$[Rh(en)_2Cl_2]NO_3$	1575	930,895	570
cis$[Rh(en)_2Cl_2]ClO_4$	1575,1625	930,895	565,555
trans$[Rh(en)_2(NH_3)Cl](NO_3)_2$	1575	930,895	575
cis$[Rh(en)_2(NH_3)Cl](NO_3)_2$	1575br	930,895	568,560
cis$[Rh(en)_2(enH)Cl]Cl_3$	1575br	925,895	570,550br
trans$[Rh(en)_2(OH_2)Cl](ClO_4)_2$	1575	930,895	570 weak
trans$[Rh(en)_2(OH_2)(NH_3)](NO_3)_3$	1575	930,895	555 weak

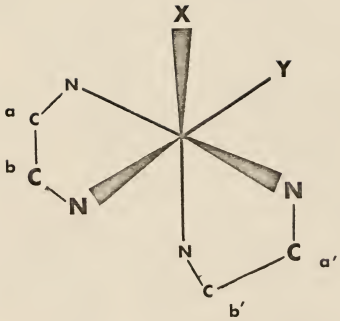

FIGURE 8 : Schematic Diagram of cis-$Rh(en)_2XY^{+n}$ For Carbon-13 nmr Chemical Shift Assignments (See Table 5).

TABLE 5. CARBON-13 CHEMICAL SHIFTS AND ASSIGNMENTS.

Compound	$\delta(^{13}C)$, ppm[a]
$Rh(en)_3^{+3}$	46.36
trans-$Rh(en)_2Cl_2^{+}$	45.68
trans-$Rh(en)_2(OH_2)Cl^{+2}$	45.75
trans-$Rh(en)_2(NH_3)Cl^{+2}$	45.64
trans-$Rh(en)_2(NH_3)(OH_2)^{+3}$	45.69

	X	Y	Assignments (see Figure 8) a	a'	b	b'
cis-$Rh(en)_2Cl_2^{+}$	Cl	Cl	46.15	46.15	47.25	47.25
cis-$Rh(en)_2(OH_2)Cl^{+2}$	Cl	OH_2	45.20	45.98	47.78	47.07
cis-$Rh(en)_2(NH_3)Cl^{+2}$	Cl	NH_3	46.27	45.81[b]	45.81[b]	47.07
cis-$Rh(en)_2(enH)Cl^{+3}$	Cl	enH	46.56	45.94[d]	45.99[d]	47.15[c]
cis-$Rh(en)_2(OH_2)(NH_3)^{+3}$	OH_2	NH_3	46.39	45.03	45.99	47.68

a) Chemical shifts reported versus TMS with dioxane (67.40 ppm) as an internal reference.

b) Peak height corresponds to two carbons, but individual peaks were not resolvable.

c) Two additional resonances at 43.30 and 40.59 ppm are assigned to the nonequivalent carbons in the ethylenediaminium ligand. The 40.59 ppm resonance is broadened, characteristic of carbons α to a quarternary nitrogen.

d) The assignments of the a' and b carbons in this complex may be reversed owing to the difficulty in predicting the effect of the small difference in chemical environment.

FIGURE 9 : Proton-decoupled C-13 Magnetic Resonance Spectra For $Rh(en)_2XY^{+n}$ Complexes.

a $Rh(en)_3^{+3}$
b <u>trans</u>-$Rh(en)_2Cl_2^{+}$
c <u>trans</u>-$Rh(en)_2Cl(OH_2)^{+2}$
d <u>trans</u>-$Rh(en)_2Cl(NH_3)^{+2}$
e <u>trans</u>-$Rh(en)_2(OH_2)(NH_3)^{+3}$
f <u>cis</u>-$Rh(en)_2Cl_2\cdot(NO_3)$
g <u>cis</u>-$Rh(en)_2Cl_2\cdot(ClO_4)$
h <u>cis</u>-$Rh(en)_2Cl(OH_2)^{+2}$
i <u>cis</u>-$Rh(en)_2Cl(NH_3)^{+2}$
j <u>cis</u>-$Rh(en)_2(enH)Cl^{+3}$ and impurities
k <u>cis</u>-$Rh(en)_2(enH)Cl^{+3}$
l <u>cis</u>-$Rh(en)_2(OH_2)(NH_3)^{+3}$

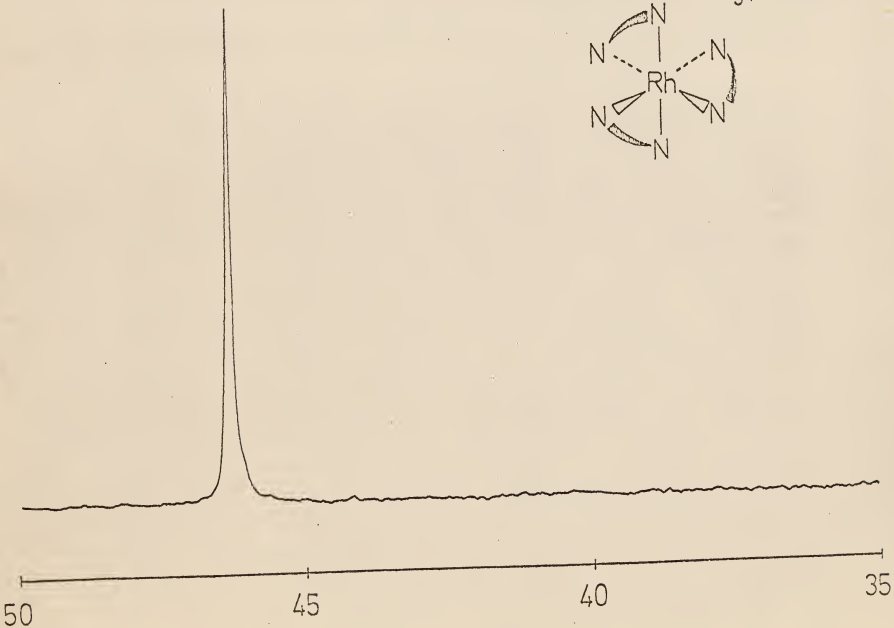
3+
N
N
N
Rh
N
N
N
50
45
40
35

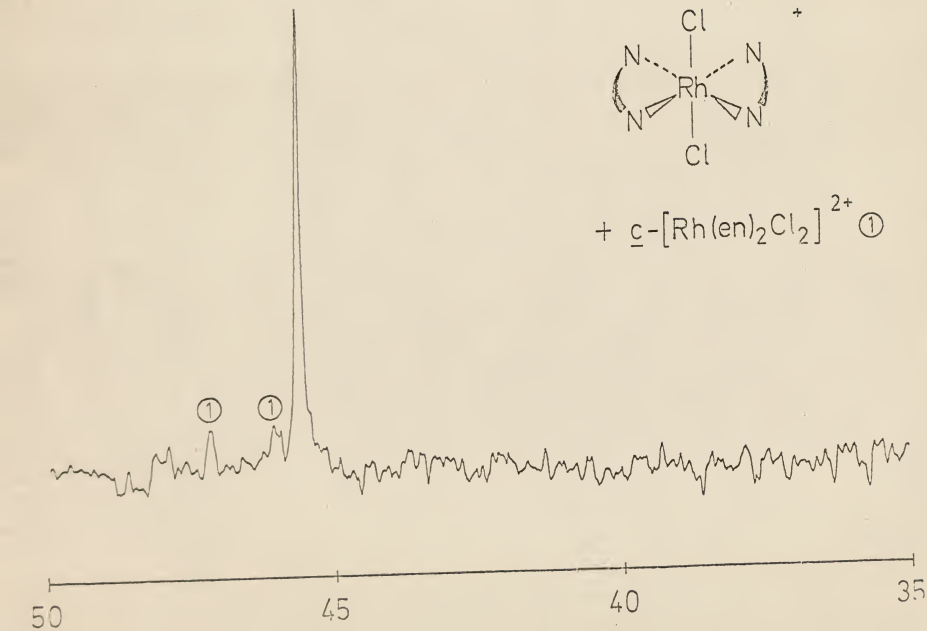
Cl
N
N
Rh
N
N
Cl
+
+ c-[Rh(en)2Cl2]2+ ①
①
①
50
45
40
35

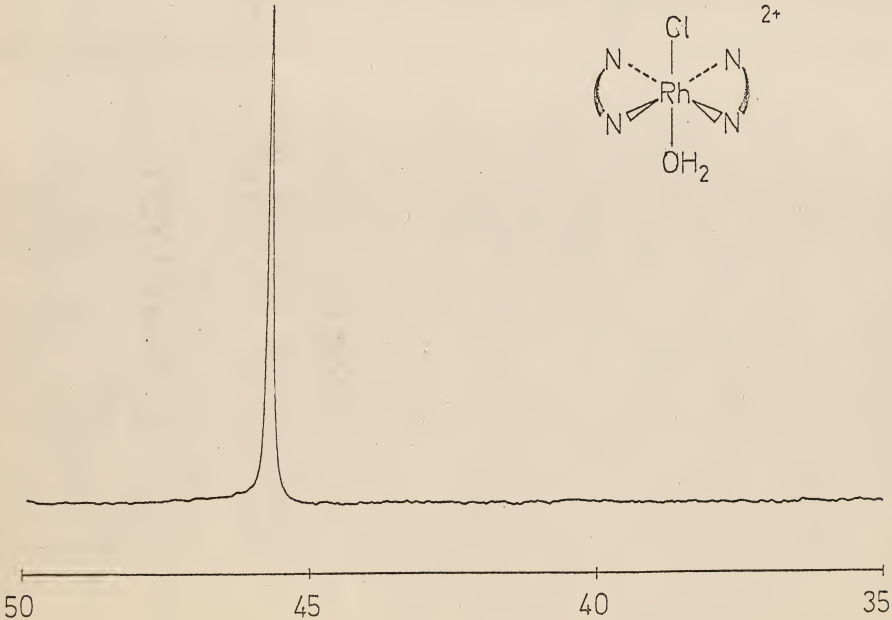
Cl
2+
N
N
Rh
N
N
OH2
50
45
40
35

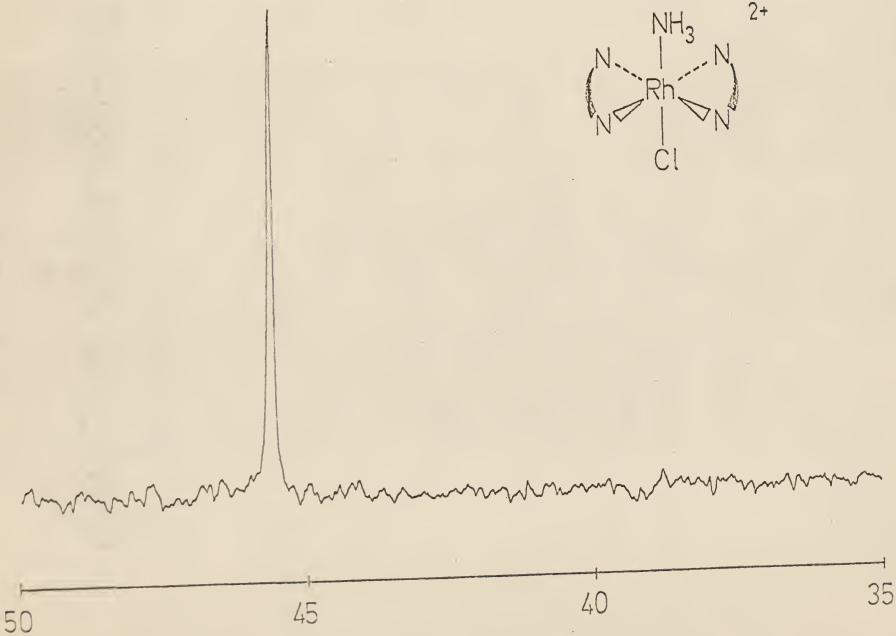
NH3
2+
N
N
Rh
N
N
Cl
50
45
40
35

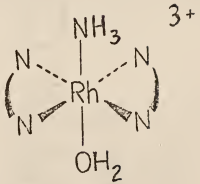
NH3
3+
N
N
Rh
N
N
OH2

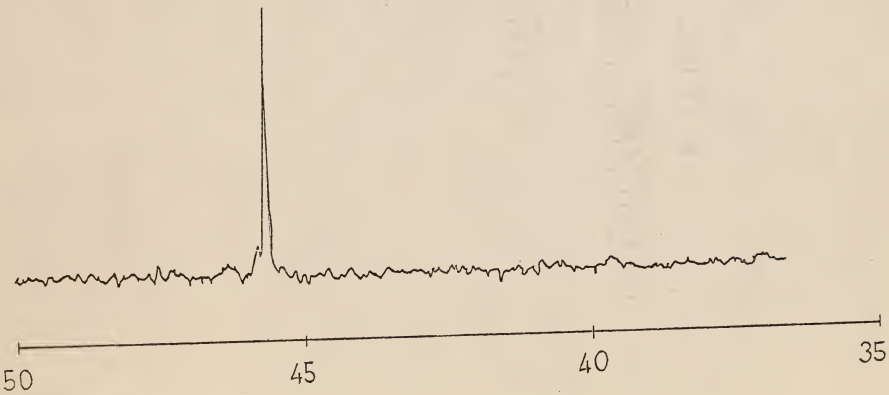
50
45
40
35

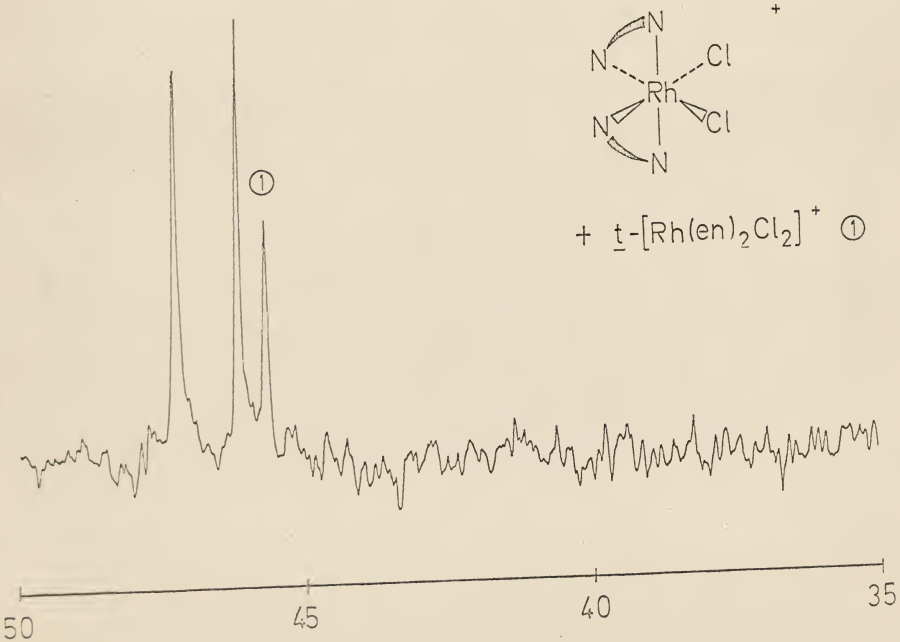
N
N
Cl
Rh
N
Cl
N
+
+ t-[Rh(en)2Cl2]+ ①
①
50
45
40
35

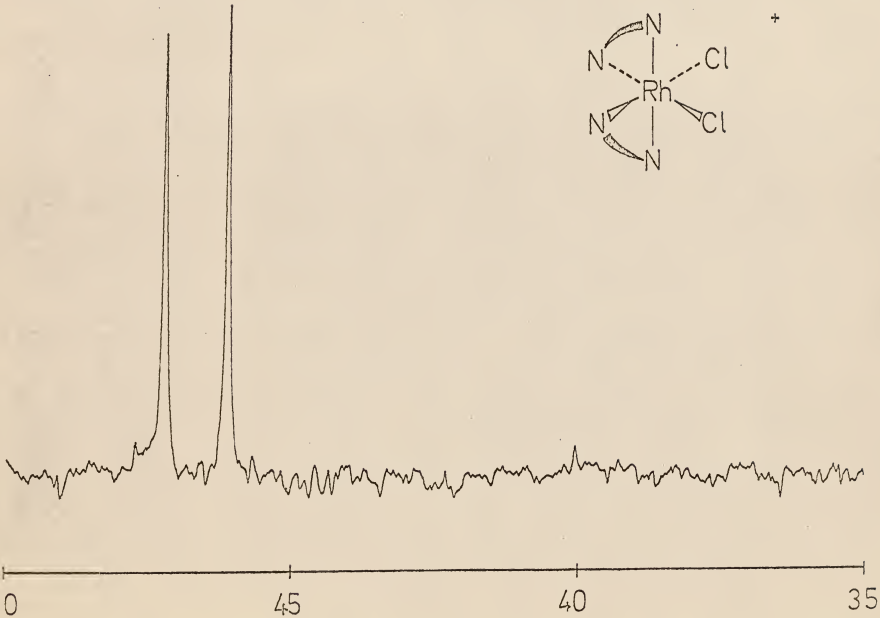
N
N
Cl
Rh
N
Cl
N
+
50
45
40
35

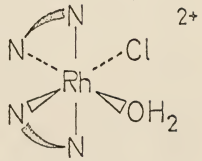
N
N
Cl
2+
Rh
N
OH2
N

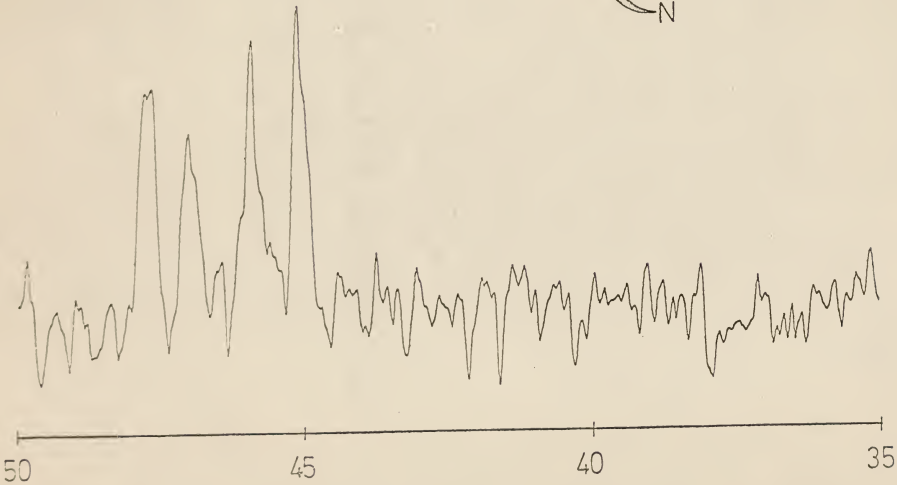
50
45
40
35

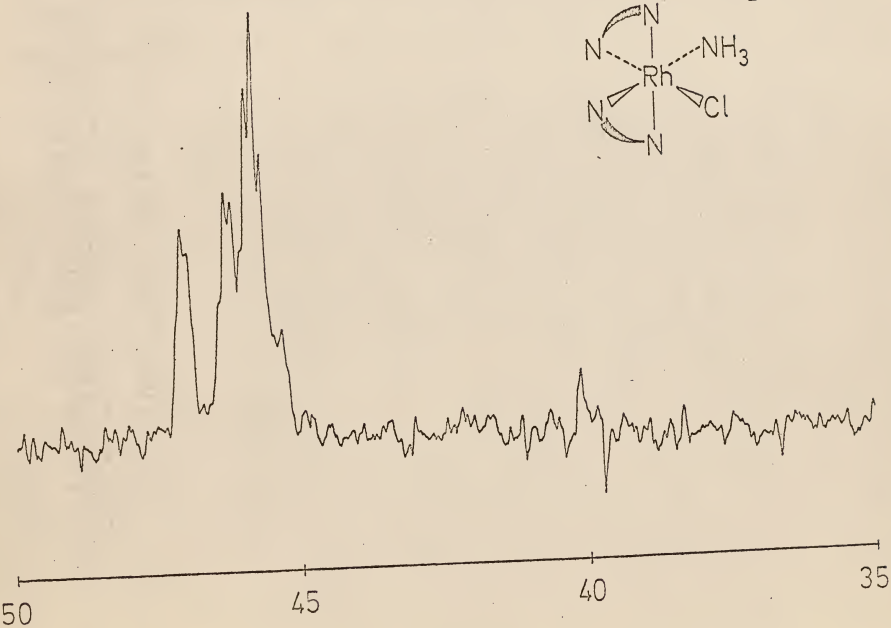
2+
N
N
NH3
Rh
N
Cl
N
50
45
40
35

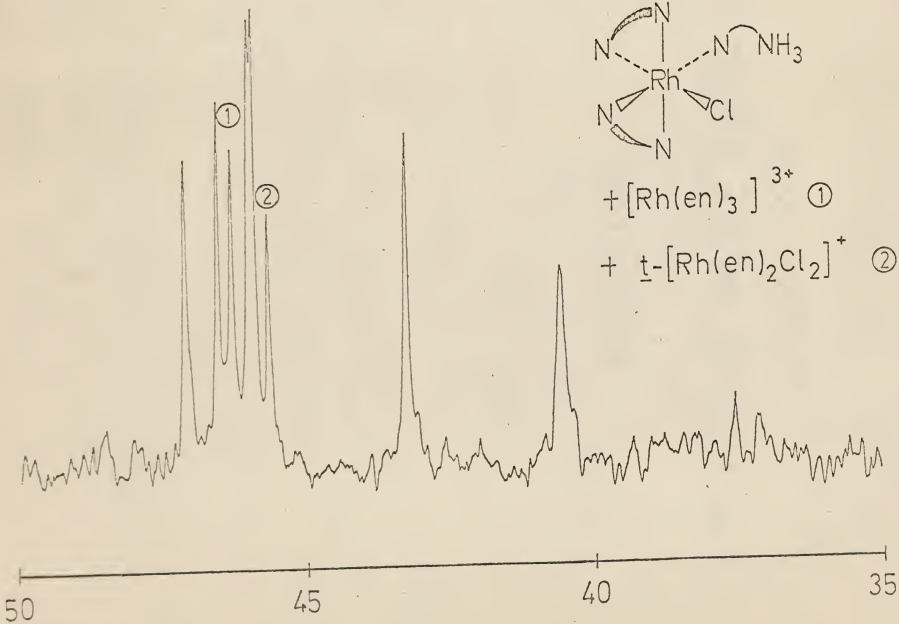
3+
N
N
N
NH3
Rh
N
Cl
N
+[Rh(en)3]3+ ①
+ t-[Rh(en)2Cl2]+ ②
①
②
50
45
40
35

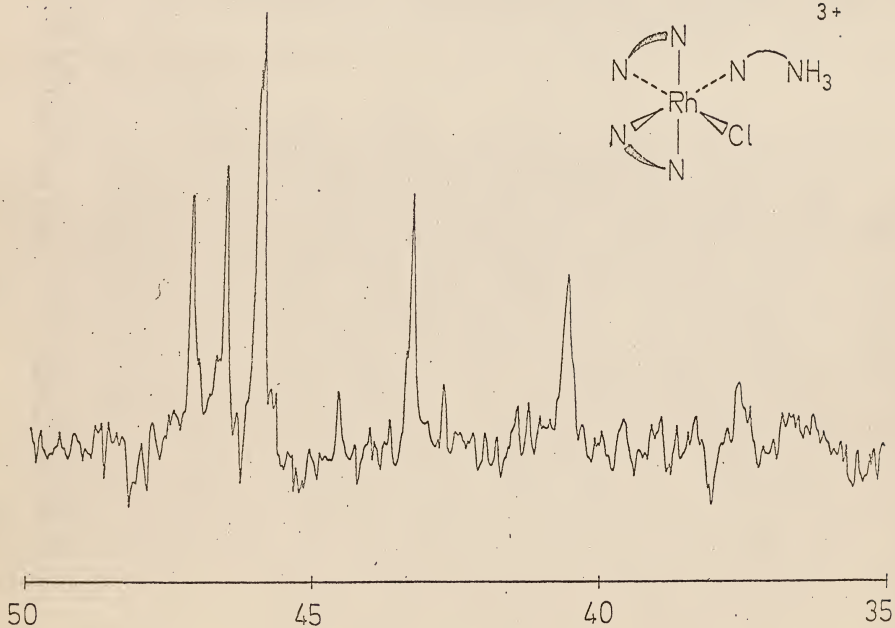
3+
N
N
N
NH3
Rh
N
Cl
N
50
45
40
35

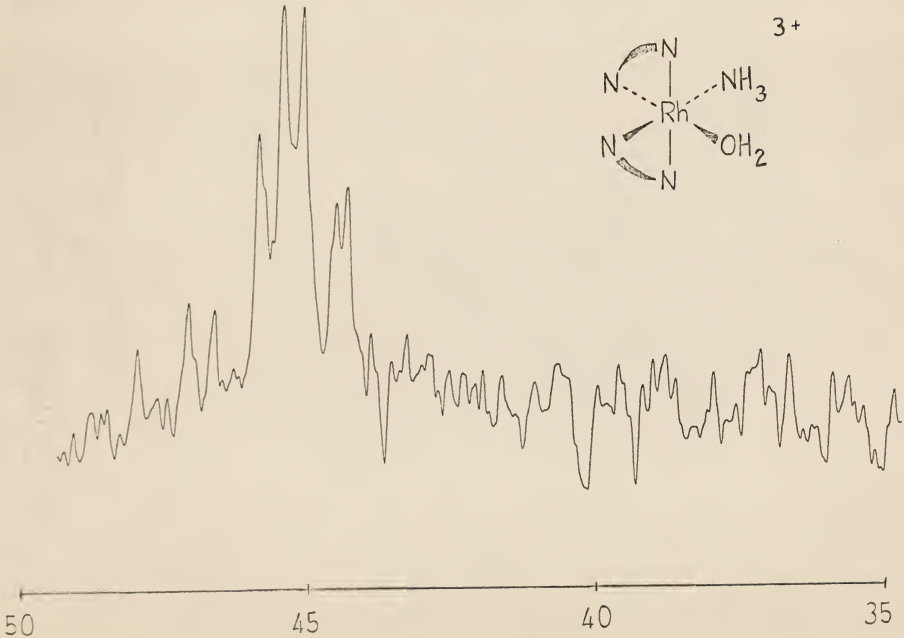
3+
N
N
NH3
Rh
N
OH2
N
50
45
40
35

C-13 nmr spectra were obtained on several complexes *in situ*. Thermally-prepared *cis*-$[Rh(en)_2(OH_2)Cl]^{+2}$, never isolated as a salt, and without any further purification, displayed four resonances in its C-13 spectrum. An extensively-photolyzed aqueous sample of $[Rh(en)_3]^{+3}$ showed six resonances attributed to the photoproduct, *cis*-$[Rh(en)_2(enH)Cl]^{+3}$, as well as two other resonances corresponding to the chemical shifts of $[Rh(en)_3]^{+3}$ and *trans*-$[Rh(en)_2Cl_2]^{+}$. Spiking the nmr sample with $[Rh(en)_3]^{+3}$ and *trans*-$[Rh(en)_2Cl_2]^{+}$ produced increased intensities at these specific resonances, confirming the exclusive formation of *cis*-$[Rh(en)_2(enH)Cl]^{+3}$ in the primary photochemical process.

An extensively photolyzed aqueous sample of *cis*-$[Rh(en)_2(NH_3)Cl]^{+2}$ displayed a complexity of resonances in the region from 45-48 ppm. The four resonances of greatest intensity are assigned to the primary photoproduct, *cis*-$[Rh(en)_2(NH_3)(OH_2)]^{+3}$, but other components in the sample produce resonances that are partially obscurred and not readily assignable. A more extensive analysis of the *cis*-$[Rh(en)_2(NH_3)Cl]^{+2}$ photochemistry and the C-13 data is found later in the discussion section.

In the C-13 nmr spectrum of *cis*-$[Rh(en)_2Cl_2]NO_3$, three resonances are observed (Fig. 9f). Resonance 1 has a chemical shift identical to the *trans*-Cl_2^{+} isomer and addition of extra *trans*-$Rh(en)_2Cl_2^{+}$ to the nmr sample tube increases the intensity of peak 1, relative to the other resonances. Reprecipitation of the NO_3^{-} salt as the ClO_4^{-} salt according to the procedure mentioned earlier, yields a C-13 spectrum of ClO_4^{-} salt

with two resonances, indicative of the selective dissolution and reprecipitation of the cis-Cl_2^+ isomer (Figure 9g).

3) Electronic Spectra - The electronic spectral data for the Rh(III) complexes is given in Table 6. The ε values listed are those reported in the references cited. In the course of this research, discrepancies were often found between the experimentally determined ε values and the literature ε values. Occassionally, these differences were attributed to a non-absorbing impurity and literature ε values were used to calculate the molar concentration of the complex.

The ε values for the cis-$[Rh(en)_2Cl_2]^+$ complex differ for the NO_3^- salt and the ClO_4^- salts, however, and the spectral differences are attributed to trans-$[Rh(en)_2Cl_2]^+$ impurity in the NO_3^- salt. Careful reprecipitation to obtain the perchlorate salt yields pure cis-$[Rh(en)_2Cl_2]^+$, as was demonstrated previously by the C-13 nmr spectrum.

Applying Beer's law to a particular wavelength, :

$$A_\lambda = l \cdot c_c \cdot \varepsilon_c + l \cdot c_t \cdot \varepsilon_t \tag{23}$$

where A_λ is the absorbance at wavelength λ, l is the cell path length, c_c and c_t are the molar concentrations of the cis- and trans- Cl_2^+ isomers, respectively, and ε's are the respective molar absorptivity coefficients at the specified wavelength.

TABLE 6. Electronic Spectra of Rh(III) Complexes

Compound	λ_{max}, nm	ε_{max}, $M^{-1}cm^{-1}$
$[Rh(en)_3]Cl_3$	301	243(238)[a]
	255	194(191)[a]
trans-$[Rh(en)_2Cl_2]NO_3$	406	83(75)[b]
	286	134(130)[b]
trans-$[Rh(en)_2(OH_2)Cl](ClO_4)_2$	386(383)[c]	55(46)[c]
	282(238)[c]	147(143)[c]
trans-$[Rh(en)_2(NH_3)Cl](NO_3)_2$	342	80(95)[b]
	275	113(120)[b]
cis-$[Rh(en)_2Cl_2]NO_3$[d]	352	147(155)[b]
	295	189(180)[b]
cis-$[Rh(en)_2Cl_2]ClO_4$	352	203
	295	205
cis-$[Rh(en)_2(OH_2)Cl]^{+2}$	325	e
	282	e
cis-$[Rh(en)_2(NH_3)Cl](NO_3)_2$	342	150[b]
	276	195[b]
cis-$[Rh(en)_2(enH)Cl]Cl_3$	345	140
	274	239

a. Reference 30.

b. Reference 31.

c. Reference 33.

d. Salt contaminated with trans-$[Rh(en)_2Cl_2]NO_3$.

e. The complex is extremely soluble in aqueous solution. Therefore, the complex salt was never isolated. The carbon-13 nmr spectrum was also recorded *in situ*.

Assuming,

$$c_{tot} = c_t + c_c, \; c_c = c_{tot} - c_t \tag{24}$$

and substituting into eq (23) above, and rearranging, we can calculate the amount of trans-Cl_2^+ impurity in the cis-$Cl_2(NO_3)$ sample.

$$C_t = \frac{A_\lambda - \ell c_{tot} t_c}{\ell(t_t - t_c)} \tag{25}$$

By the above spectral analysis, the cis-Cl_2^+ nitrate salt, prepared by the standard literature procedure of Johnson and Basolo,[31] is found to contain as much as 20% trans-Cl_2^+ impurity.

The cis-$[Rh(en)_2Cl_2]^+$ perchlorate salt also undergoes isomerization in the solid state as evidenced by spectroscopic (UV) changes occurring within approximately three weeks time (Fig. 10).[35] Removal of the trans-$Rh(en)_2Cl_2^+$ impurity prior to the photochemical study of the cis-Cl_2^+ complex was not necessary, however, because of the relatively inefficient chemical activity of the trans-$[Rh(en)_2Cl_2]^+$ relative to that of cis-$[Rh(en)_2Cl_2]^+$.

Photochemical Data

Tables 7 and 8 and Appendix 2 contain the photochemical data for all the Rh(III) complexes investigated. The quantum yields are absolute values for product formation and were determined by analysis of the spectral changes occurring upon photolysis (see Experimental).

FIGURE 10 : UV Spectra of Thermally Prepared[31] cis-$Rh(en)_2Cl_2^+$ Nitrate (----) and Perchlorate (----) Salts (See Table 6)

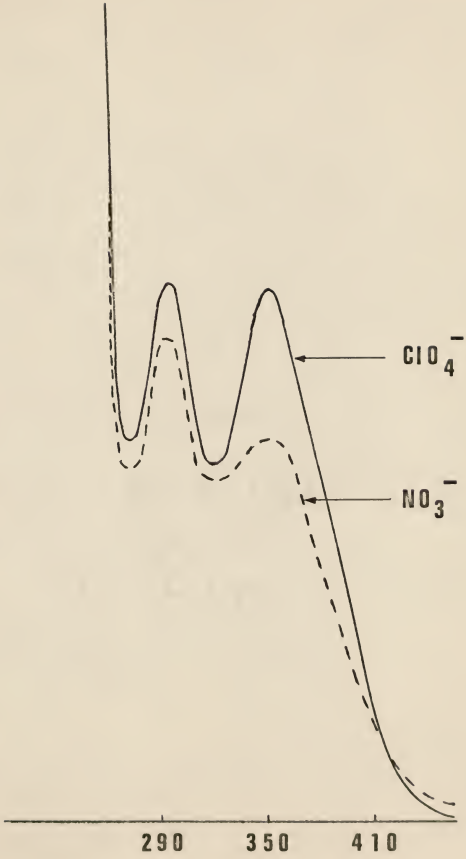
ClO_4^-
NO_3^-
290
350
410

TABLE 7. QUANTUM YIELDS FOR LF PHOTOLYSIS OF Rh(III) AMINES.

Compound	$\lambda_{irr.}$ nm	Φ_{H_2O}, moles/einst.	Photoproduct
<u>cis</u>-$Rh(en)_2Cl_2^{+}$ [a]	365	0.43 ± 0.02(4)	<u>trans</u>-$Rh(en)_2(OH_2)Cl^{+2}$
<u>trans</u>-$Rh(en)_2Cl_2^{+}$ [a]	405	0.061 ± 0.003(4)	<u>trans</u>-$Rh(en)_2(OH_2)Cl^{+2}$
<u>cis</u>-$Rh(en)_2(NH_3)Cl^{+2}$ [a]	365	0.145 ± 0.006(4)	<u>cis</u>-$Rh(en)_2(NH_3)(OH_2)^{+3}$
<u>trans</u>-$Rh(en)_2(NH_3)Cl^{+2}$ [a]	365	0.062 ± 0.0007(6)	<u>trans</u>-$Rh(en)_2(NH_3)(OH_2)^{+3}$
<u>trans</u>-$Rh(en)_2(NH_3)(OH_2)^{+3}$ [a,b]	313	not measured	<u>trans</u>-$Rh(en)_2(NH_3)(OH_2)^{+3}$

Quantum yields reported for the formation of photoproduct are mean values with average deviations. Number of determinations are in parentheses.

a) Aqueous 0.014 <u>N</u> $HClO_4$, 25°C, 6 ml 2.0 cm cells.

b) UV spectrum (450-250 nm) of sample showed slight changes after 30 minutes irradiation time. An additional 27 hours of irradiation produced no further spectral changes.

TABLE 8. PHOTOCHEMICAL QUANTUM YIELDS FOR THE FORMATION OF *cis*-$Rh(en)_2(enH)Cl^{3+}$ at 313 nm (1*M* Cl^-, 25°C)

pH	$\Phi_{formation}$[a]
0	0.041 ± 0.004(4)
2	0.042 ± 0.006(5)
4	0.045 ± 0.003(2)
6	0.037 ± 0.003(2)
8	0.038 ± 0.007(2)
10	0.039 ± 0.003(2)[b]
12	0.035 ± 0.01 (2)[c]

a. Quantum yield (initial) for formation of *cis*-$Rh(en)_2(enH)Cl^{3+}$, mean value and average deviation reported with number of determinations in parentheses.

b. Shifting of isosbestic pts. at 263 and 244 nm.

c. Loss of isosbestic points.

Trans-$[Rh(en)_2Cl_2]^+$, irradiated at 405 nm in aqueous 0.014 N $HClO_4$, yields exclusively trans-$[Rh(en)_2(OH_2)Cl]^{+2}$ with a quantum efficiency of 0.061. This result is consistent with a previously reported value of 0.057.[36] Muir and Huang[28] obtained a quantum yield for aquation of 0.030, but they irradiated at a wavelength of 254 nm, and also, their difficulty in determining absolute quantum yields leads one to doubt their quantitative data.

Trans-$[Rh(en)_2(NH_3)Cl]^{+2}$, irradiated at 365 nm in aqueous 0.014 N $HClO_4$, yields exclusively trans-$[Rh(en)_2(NH_3)(OH_2)]^{+3}$ with a quantum efficiency of 0.062. The exclusive photoaquation of the chloride ligand represents analogous behavior to the chloropentaammine Rh(III) system.[22]

Ligand field irradiation (313nm) of trans-$Rh(en)_2(NH_3)(OH_2)^{+3}$ initially produces small spectral changes, attributed to reactive impurities. Upon extended irradiation (24 hours), however, no further spectral changes occur. Stereoretentive aquo ligand exchange is believed to be the exclusive photosubstitution reaction and hence, electronic spectral characteristics are preserved. Again, this reaction is analogous to the $[Rh(NH_3)_5(OH_2)]^{+3}$ photoexchange reaction[29] which was studied using 18_O labeled water, but no quantum yield data was obtained for the trans-$[Rh(en)_2(NH_3)(OH_2)]^{+3}$ photochemistry.

$[Rh(en)_3]^{+3}$, irradiated at 313 nm in aqueous 1 M Cl^- and at various proton concentrations (pH=0-8), labilizes one end of an ethylenediamine and Cl^- ligand coordinates to yield exclusively cis-$[Rh(en)_2(enH)Cl]^{+3}$ (Table 8). The cis configuration was

deduced from the photon-decoupled C-13 nmr spectrum of the photolyzed sample, discussed below. The pH-independent (pH 0-8) quantum yield for product formation is 0.04 moles/einstein. Although this reaction represents photoanation as opposed to photoaquation in the previous three reactions, the 100% stereoretentive process is consistent with the stereorigidity, observed thus far in the Rh(III) amine photosubstitution reactions.

The difference spectrum shown in Figure 11 was obtained at pH 2 and the total irradiation time was restricted in order to limit the reaction to 20% for the purpose of quantum yield calculations. The isosbestic points in the difference spectrum indicate only primary photochemical processes occurring during the course of the experiment. Although the photoproduct is thermally stable in solution at room temperature, it undergoes a secondary photochemical process to form trans-$[Rh(en)_2Cl_2]^+$, evidenced by the growth of an absorption band at 406 nm.

Cis-$[Rh(en)_2Cl_2]^+$, irradiated at 365 nm in aqueous 0.014N $HClO_4$, yields exclusively trans-$[Rh(en)_2(OH_2)Cl]^{+2}$ with a quantum yield of 0.43. (Table 7) The stereochemistry of the product is consistent with Muir and Huang's observations, although the quantum efficiency for substitution is considerably greater than their result (0.056 moles/einstein[28]).

Cis-$[Rh(en)_2(NH_3)Cl]^{+2}$, irradiated at 365 nm in aqueous 0.014N $HClO_4$, undergoes photoaquation to yield predominantly cis-$[Rh(en)_2(NH_3)(OH_2)]^{+3}$ with a quantum yield of 0.145 moles/einstein.

FIGURE 11 : UV Difference Spectrum. Photolysis Sample vs. Dark Reference as a Function of Irradiation Time for the Irradiation of $Rh(en)_3^{3+}$ at 313 nm. Positive Absorbance changes at 350 nm are Due to Formation of the Photolysis Product, cis-$Rh(en)_2(enH)Cl^{3+}$. Negative absorbance changes at ~255 and ~305 nm are Due to Depletion of Starting Material, $Rh(en)_3^{3+}$.

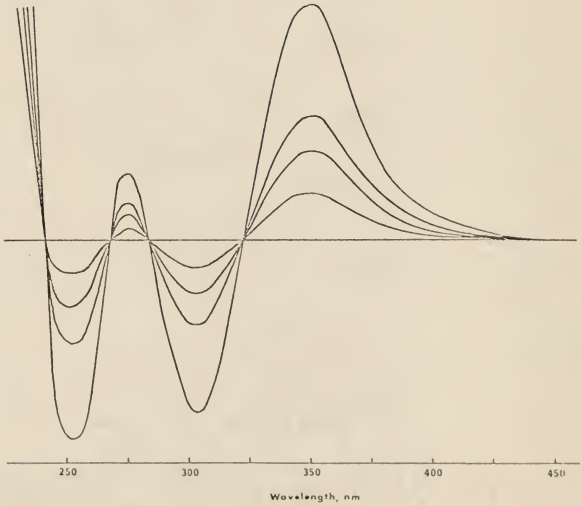
250
300
350
400
450
Wavelength, nm

Labilization of Cl^- is consistent with the LF reactivities of $[Rh(NH_3)_5Cl]^{+2}$ [22] and trans-$[Rh(en)_2(NH_3)Cl]^{+2}$. The photoaquation of cis-$[Rh(en)_2(NH_3)Cl]^{+2}$ may not be 100% stereoretentive, since the C-13 nmr spectrum of the photolyzed sample contains several unassigned resonances (see C-13 section).

DISCUSSION

As outlined earlier (see introduction), Adamson's Rules cannot be used successfully to explain the general photochemical reactivity of hexacoordinate rhodium(III) amine complexes. Our results concur with this conclusion (Tables 7 and 8) and necessitate the development of a new mechanistic approach that not only accounts for which ligand is labilized, but also rationalizes the stereochemistry of the reaction products.

Nature of the Labilized Ligand

The nature of the labilized ligand for all the reactions studied in this research can be explained through the use of the Angular Overlap Model (AOM)[37] and a molecular orbital approach developed by Zink.[38] AOM is an approximate mo technique that determines relative molecular orbital energy levels through a geometric analysis of metal orbital and ligand orbital overlap. The secular determinants, constructed through AOM, for several five- and six-coordinate species are given in Appendix 3. The letter "e" with indices σ, π_x or π_y symbolizes the unit energy change obtained when the geometry is ideal for bond formation, i.e.,when the overlap integral in question is maximum. The diagonal elements of the matrix represent the energies of that particular mo when all off-diagonal elements are zero. A non-zero off-diagonal element indicates mixing of metal d orbitals, and the mo's (linear combinations of the d orbitals involved) are at different energies than indicated by the diagonal elements. For this discussion, however, an approximation regarding molecular

orbital energy levels will be adopted, and the diagonal elements for all species will represent the energies of the mo's.

For the general species, trans-$[Rh(en)_2XY]^{+n}$, where X and Y are ligands of lower or equal ligand field strength to ethylenediamine, the lowest energy LF transition represents promotion of an electron from the degenerate d_{xz},d_{yz} set to the d_{z^2} orbital. A first-order Jahn-Teller distortion of the molecule will occur to remove the degeneracy of the d_{xz}, d_{yz} orbitals (Figure 12), and this is discussed below in terms of the sterochemistry of the reaction. If one of the axial ligands has filled π orbitals (e.g. Cl^-), the loss of electron density from the (π antibonding) d_{xz}, d_{yz} pair will result in a strengthening of the π bonding in the z direction; the increase of electron density in the -antibonding d_{z^2} orbital weakens the σ bonding in the z direction. The net effect on the bonding will depend on the relative strengths of the σ and π interactions of the ligand since the σ weakening and π strengthening oppose each other in this case. For most ligands, however, the σ effect will dominate and preferential ligand labilization should occur along the z axis, thus, trans-$[Rh(en)_2Cl_2]^+$ undergoes exclusive photoaquation of Cl^- to yield trans-$[Rh(en)_2(OH_2)Cl]^{+2}$.

When X and Y are different ligands, the weaker of the two metal-ligand bonds in the ground state remains the weaker bond in the electronic excited state. The ligand with the weaker metal-ligand bond is preferentially labilized. Thus, trans-$[Rh(en)_2(NH_3)Cl]^{+2}$ undergoes exclusive photoaquation of Cl^- to yield trans-$[Rh(en)_2(NH_3)(OH_2)]^{+3}$, and trans-$[Rh(en)_2(NH_3)(OH_2)]^{+3}$ presumably undergoes aquo

ligand exchange, which is consistent with the lack of spectral changes after photolysis.

A similar approach can be used to explain the LF activity of the cis-$[Rh(en)_2XY]^{+n}$ complexes (Appendix 3 and Figure 12). The lowest energy LF transition promotes an electron from the d_{xy} mo to the $d_{x^2-y^2}$ mo. The increased σ antibonding character favors labilization in the xy plane, and, as noted for the trans apecies, the ligand less strongly bound to the metal is preferentially labilized. This conclusion is confirmed by the experimental data for both cis-$[Rh(en)_2Cl_2]^+$ and cis-$[Rh(en)_2(NH_3)Cl]^{+2}$, which undergo photoaquation of Cl^- to yield trans-$[Rh(en)_2(OH_2)Cl]^{+2}$ and cis-$[Rh(en)_2(NH_3)(OH_2)]^{+3}$, respectively.

$Rh(en)_3^{+3}$ undergoes photoanation in the presence of Cl^- to yield cis-$[Rh(en)_2(enH)Cl]^{+3}$, when irradiated in its lowest energy LF band. If one assumes O_h site symmetry, promotion of an electron from the t_{2g} (π non-bonding) set to the e_g (σ antibonding) set increases σ antibonding character in the molecule, and favors labilization along any one of the three indistinguishable molecular axes.

LF Photochemistry of trans-$[Rh(en)_2XY]^{+n}$

While the above molecular orbital treatment justifies the preferential ligand labilization, this approach must be extended to account for changes occurring in the formation of the photoproduct. That is, one must consider the five-coordinate intermediate (its geometry and reactivity) to account for the stereospecificity of these photochemical reactions.

Both trans-$Rh(en)_2Cl_2^+$ and trans-$Rh(en)_2(NH_3)Cl^{+2}$ undergo photoaquation of Cl^- when irradiated in their lowest energy LF band. As shown earlier, the electronic configuration for this excited state, under C_{4v} symmetry, is Jahn-Teller unstable. A spontaneous distortion of the molecule will occur to remove the J-T degeneracy (Figure 12). As Cl^- leaves, the two equatorial nitrogen atoms in the xz plane fold down, and as a result of this distortion, the dxz and dyz orbitals are no longer a degenerate pair. The motion of the nitrogen atoms may be thought of as "following" the chloro ligand. A similar mechanism applies to the photolysis of trans-$Rh(en)_2(NH_3)(OH_2)^{+3}$, where aquo ligand is the proposed leaving group.

In Figure 12a, the five-coordinate species approaches the trigonal-bipyramidal geometry with the X ligand occupying an equatorial site. AOM calculations on the square pyramidal excited configuration and the trigonal bipyramidal structure obtained by moving the x-axis nitrogen atoms in the negative z direction (Figure 12a) indicate that the square pyramidal structure is more stable than the TBP geometry. The trigonal bipyramidal intermediate can also be formed by rearrangement of a square pyramidal species containing X in the equatorial plane (later in this section). If the distortion in Figure 12a goes all the way to the trigonal bipyramidal structure, we might expect a nearly statistical ratio os cis and trans products. However, trans-$Rh(en)_2(OH_2X^{n+}$ is the only product formed for X = NH_3 and Cl. Apparently aquo ligand addition to form the photoproduct takes place prior to formation of the trigonal bipyramidal structure and further rearrangement to yield square pyramidal intermediates with X in the equatorial plane.

FIGURE 12 : Molecular Orbital Representation of Ligand Field Excitation and Spontaneous Jahn-Teller Distortion of <u>trans</u>-$Rh(en)_2XCl^{+n}$ (Part A) and <u>cis</u>-$Rh(en)_2XCl^{+n}$ (Part B)

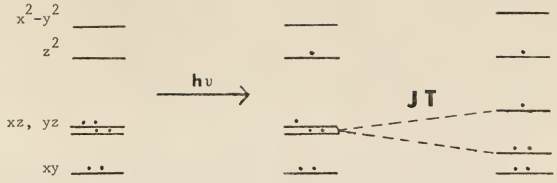
x2-y2
z2
hυ
JT
xz, yz
xy

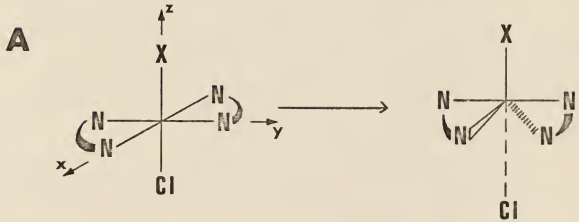
A
z
X
N
N
N
N
N
N
y
x
Cl
X
N
N
N
N
Cl

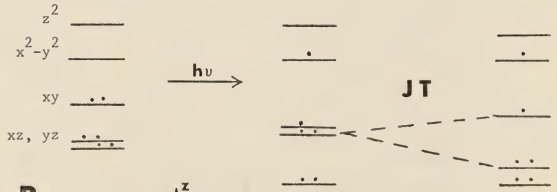
z2
x2-y2
hυ
JT
xy
xz, yz

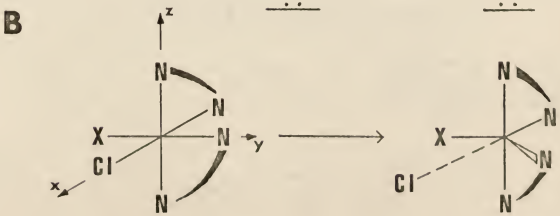
B
z
N
N
X
N
y
Cl
x
N
N
N
X
N
Cl
N

LF Photochemistry of cis-$[Rh(en)_2XY]^{+n}$

Cis-$[Rh(en)_2Cl_2]^+$, when irradiated in its lowest energy LF band, yields 100% trans-$[Rh(en)_2(OH_2)Cl]^{+2}$, as confirmed by electronic spectral changes and C-13 nmr spectroscopy. The photochemical reaction of the cis-Cl_2^+ species, when first studied by Muir and Huang,[28] represented unique behavior in the Rh(III) amines. Thermally, aquation of chloride is stereoretentive to yield exclusively cis-$[Rh(en)_2(OH_2)Cl]^{+2}$ [31] (see Experimental). Photochemically, the efficient rearrangement of ligands in the five-coordinate intermediate to result in an exclusive trans product is reminiscent of Cr(III) photoreactivity, but not very common in d^6 systems.

Three possible mechanistic interpretations may be proposed to explain the LF reactivity of cis-$[Rh(en)_2Cl_2]^+$:

(1) LF labilization of one end of an ethylenediamine ligand, which then "edge displaces" chloride, and aquation occurs trans to Cl^-;

(2) Photoisomerization of cis-Cl_2^+ to trans-Cl_2^+, followed by photoaquation of the trans-Cl_2^+ species;

(3) LF labilization of Cl^-, followed by rearrangement of the five-coordinate intermediate, and aquation occurring trans to Cl^-.

Mechanisms (1) and (2) were initially proposed by Muir and Huang[28]. The first mechanism is an adaptation of Adamson's rules[12], which predicts preferential labilization of the strong-field ligand (N of ethylenediamine) along the average weak-field axis (indicated by dashed lines in equation 29). By an edge displacement process

(see Cr(III) photochemistry in Introduction), a chloro ligand is forced

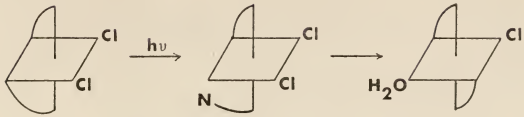

(29)

out of its coordination site and aquation occurs at the initial site of labilization. In lieu of the results for the LF photolysis of $Rh(en)_3^{+3}$ (discussed later), where the stable cis-$[Rh(en)_2(enH)]^{+3}$ species is formed even in mildly basic solution, it is doubtful that the above mechanism is correct. Under the acidic conditions (pH ∿2) of this reaction[28], a labilized amine ligand should be protonated and not recoordinate via edge displacement of chloro ligand.

The second mechanism, proposing an initial cis → trans photomerization, followed by the stereoretentive photoaquation of trans-$[Rh(en)_2Cl_2]^+$ to yield trans-$[Rh(en)_2(OH_2)Cl]^{+2}$, was postulated by Muir and Huang because of the detection of trans-$[Rh(en)_2Cl_2]^+$ in a photolyzed sample of cis-$[Rh(en)_2Cl_2]^+$.[28] From our C-13 nmr spectra and discrepancies in molar absorptivity coefficients (Table 6), we can account for the presence of the trans-Cl_2^+ isomer as an impurity in the starting material, and not as a photochemically-generated species (discussed later in the nmr section). Also, since the photosubstitution quantum yield (Φ = 0.43) for the cis-$[Rh(en)_2Cl_2]^+$ complex ion is considerably greater than the quantum yield (Φ = 0.061) for the trans isomer, photoisomerization cannot possibly be a preliminary process to photosubstitution.

The third mechanism best accounts for the reactivity observed for the general compounds, cis-$Rh(en)_2XCl^{n+}$ (where X = NH_3, Cl). It is also consistent with recent work by Strauss and Ford[27] in which photolysis of cis-$Rh(NH_3)_4XY^{2+}$ (X = Cl, H_2O and Y = Cl, H_2O) resulted in trans-tetraammine products. Irradiation of cis-$Rh(en)_2Cl_2^+$ at 365 nm leads to chloro ligand loss and presumably the initial formation of a square pyramidal five-coordinate intermediate with an equatorial chloro ligand. If the five-coordinate intermediate assumes a trigonal bipyramidal geometry, a Jahn-Teller distortion of the molecule will occur to remove the orbital degeneracy (Figure 12b). Since LF photolysis of cisRh$(en)_2Cl_2^+$ yields exclusively trans-$Rh(en)_2(OH_2)Cl^{+2}$, facile rearrangement of the trigonal bipyramid to the more stable square pyramid (Cl^- axial) must take place prior to aquation. (The relative stabilities of the two limiting geometries is confirmed by a calculation of their orbital stabilization energies via AOM (see Appendix 3). The AOM model calculates the two ground state square pyramidal geometries (Cl^- axial, Cl^- equitorial) as equal in energy, but for the lowest energy LF excited state, the square pyramid (Cl^- axial) geometry is more stable by an energy difference of $3/4(e^{N}-e^{Cl})$. Also, if one assumes that chloride labilization is the only structural perturbation in the LF photolyses of both cis- and trans-$Rh(en)_2XCl^{+n}$, then the square pyramid (X equatorial) geometry lies at higher energy than the square pyramid (X axial) geometry. This conclusion is based on the relative energies of the ligand field excited states for the parent compounds (Figure 13).

Cis-$Rh(en)_2(NH_3)Cl^{+2}$ undergoes photoaquation to yield predomi-

FIGURE 13 : Schematic Potential Energy Diagram Depicting the Stereochemical Course of a Photosubstitution Reaction Upon Population Into a Ligand Field (LF) Excited State.

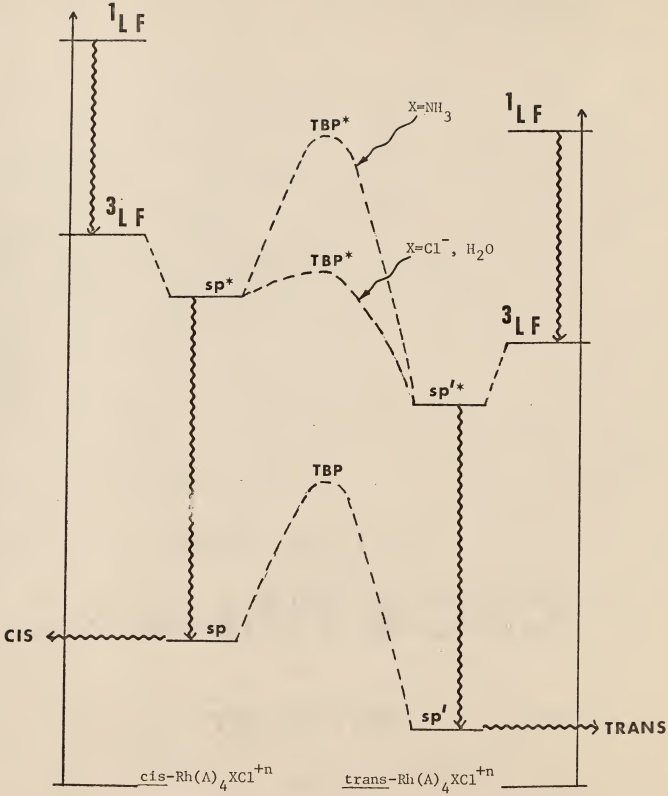
^{1}LF
^{3}LF
TBP*
X=NH$_3$
^{1}LF
X=Cl$^-$, H$_2$O
TBP*
sp*
^{3}LF
sp'*
TBP
CIS
sp
sp'
TRANS
cis-Rh(A)$_4$XCl^{+n}
trans-Rh(A)$_4$XCl^{+n}

nantly cis-$[Rh(en)_2(NH_3)(OH_2)]^{+3}$, with some trans isomer also possibly formed.

Figure 13 schematically explains the photochemical behavior of both the cis- and trans-$[Rh(en)_2XCl]^{+n}$ complexes (X = Cl, NH_3).[27] Both cis complexes (X = Cl, NH_3), when excited into a singlet ligand field excited state, undergo intersystem crossing to ^3LF,[26] and labilize Cl^- to form the five-coordinate excited state square pyramidal species, sp*, where ligand X assumes an equatorial position. There is a certain activation energy required for converting from the square pyramid (Cl^- equatorial) to the square pyramid (Cl^- axial), sp'*, with the trigonal bipyramidal geometry, TBP*, near the transition state. When X = Cl^-, this energy barrier is small and facile conversion to the sp'* excited state takes place, enabling exclusive trans aquation to occur. When X = NH_3, the energy barrier to TBP* is considerably larger, and hence, aquation preferentially occurs prior to rearrangement of the five-coordinate species, i.e. cis to NH_3.

Ligand field excitation of the trans-$[Rh(en)_2ClX]^{+n}$ (X = Cl^-, NH_3) species results in exclusive labilization of chloro ligand, and and an excited state five-coordinate intermediate. The five-coordinate species initially assumes a square pyramidal geometry with the X ligand occupying an axial site (sp'*). Whether X = Cl^- or NH_3, the activation energy barrier is too large for facile rearrangement to the TBP* structure. Hence, aquation occurs via a stereoretentive process.

This diagram is consistent with the LF photochemistry of the cis- and trans-$[Rh(NH_3)_4(OH_2)X]^{+n}$ (X = Cl^-, OH_2) complexes,[27] whereby the cis species yield trans$[Rh(NH_3)_4(OH_2)X]^{+n}$ and the trans isomers appear to undergo stereoretentive aquo ligand exchange. Similar to the $[Rh(en)_2Cl_2]^+$ case, the square pyramid (H_2O equatorial) excited state geometry (formed from the LF photolysis of the cis isomer) easily surmounts a small activation barrier for rearrangement and aquation occurs after rearrangement. The square pyramid (H_2O axial) excited state geometry (formed from the LF photolysis of the trans isomer), however, is confronted by a large activation barrier, and therefore, aquation occurs prior to rearrangement.

LF Photochemistry of $Rh(en)_3^{+3}$

$Rh(en)_3^{+3}$, when irradiated at 313 nm in the presence of H^+ and 1M Cl^-, yields the thermally stable (@ 25°C) cis-$[Rh(en)_2(enH)Cl]^{+3}$. The postulation of cis-$[Rh(en)_2(enH)Cl]^{+3}$ as the photoproduct is made on the basis of the following considerations:

1) The similarity in the electronic band maxima between the photoproduct and $[Rh(NH_3)_5Cl]^{+2}$ suggests that five amine groups and one chloro group are bound to Rh(III) in the photoproduct. (The product is not formed in chloride-free solutions.)

2) The spectroscopic determination of moles of photolysis product versus moles of protons consumed (measured by pH change) corresponds to a 1:1 ratio (Table 9). This data is consistent with a mono-protonated ethylenediamine in the photolysis product.

3) Elemental analysis is most consistent with four chlorides per Rh(III) metal atom which suggests either an ethylenediaminium

ligand, or an HCl of solvation is present in the isolated salt.

4) When a mixture of $Rh(en)_3^{+3}$ and the photoproduct are passed through an ion-exchange column (Dowex 50W X-4), both species are eluted together (2.5M HCl). This implies that both ions have a +3 charge.

5) The photoproduct at pH8 is identical spectroscopically to the product at pH0. At 1M H^+ concentration, any non-coordinated aliphatic primary amines should be protonated.

6) The cis geometry for $[Rh(en)_2(enH)Cl]^{+3}$ is assigned on the basis of the proton-decoupled, carbon-13 nmr spectrum (Figure 9k). Six lines are observed for the six chemically unique carbon atoms at 47.15, 46.57, 46.00, 45.94, 43.30 and 40.59 ppm. A discussion and more detailed analysis of the C-13 nmr spectrum for the photoproduct is presented later in the C-13 nmr section.

The quantum yields for the formation of cis-$[Rh(en)_2(enH)Cl]^{+3}$ at 313 nm in aqueous 1M Cl^- solutions are independent of proton concentration ($0 \leq p \leq 8$)(Table 8). Figure 11 displays a typical photolysis sample versus thermal sample reaction plot for various irradiation times. The longest irradiation time corresponds to approximately 20% reaction. Isobestic points (323, 285, 267 and 244 nm) indicate that no secondary photochemical or thermal reactions of the product are taking place during the first 20% of the reaction. The increases and decreases in absorbance occur at wavelengths corresponding approximately to the maxima of the photoproduct and the starting material, respectively. When a 2.5×10^{-3}M solution (pH2, 1M Cl^-) of $Rh(en)_3^{+3}$ is photolyzed to

>90% reaction, the resulting solution has bands at 345 and 278 nm with molar absorptivity coefficients (after attempting to correct for the unreacted $Rh(en)_3^{+3}$ and a small amount of trans-$[Rh(en)_2Cl_2]^+$ formed via a secondary photochemical process) of 132 and 197 M^{-1} cm^{-1}, respectively. The extinction coefficient at 345 nm is within 6% of the value listed in Table 6 for cis-$[Rh(en)_2(enH)Cl]^{+3}$. Corrections were made spectroscopically by Gaussian curve shape analysis. Concentrations of trans-$[Rh(en)_2Cl_2]^+$ (5-7%) were determined from a well defined shoulder at 406 nm, while concentrations of $Rh(en)_3^{+2}$ (<2%) were calculated from a very small shoulder on the long wavelength side of the 277 nm band in the photolysis product.

The 1:1 ratio of the formation of cis-$[Rh(en)_2(enH)Cl]^{+3}$ to the consumption of protons (Table 9), and the presence of isosbestic points during the photolysis reaction (Figure 11), indicate that the quantum yield for formation of cis-$[Rh(en)_2(enH)Cl]^{+3}$ is equal to the quantum yield for formation of cis-$[Rh(en)_2(enH)Cl]^{+3}$ is equal to the quant· yield for degradation of $Rh(en)_3^{+3}$ in acidic chloride media. 1M chloride is an efficient scavenger for the open coordination site, even when competing with ∿55 M water. Monacelli[39] has shown that the ion-pair equilibrium constant for the +3- charged species, $[Rh(NH_3)_5(OH_2)]^{+3}$,[29] in 1M Cl^- is $0.16M^{-1}$. Data on the photoaquation of $[Rh(NH_3)_5(OH_2)]^{+3}$ [29], in 1M Cl^-, indicate that 63% of the $[Rh(NH_3)_5Cl]^{+2}$ formed occurs via an exchange in the ion-pair and the quantum yield for the photoexchange of the ion-pair is close to unity. The extensive ion-pair formation can explain the exclusive formation of cis-$[Rh(en)_2(enH)Cl]^{+3}$; the proximity of the two ions enables Cl^- coordination

TABLE 9. SIMULTANEOUS DETERMINATION FOR THE PHOTOCHEMICAL FORMATION OF cis[Rh(en)$_2$(enH)Cl]$^{+3}$ AND CONSUMPTION OF PROTONS.

Exp.	$Rh(en)_3^{+3}$, initial[a]	cis-$Rh(en)_2(enH)Cl^{+3}$, final[b]	H^+, initial[c]	H^+, final[d]	H^+, consumed[e]
1	14.0	1.8	4.6	2.7	1.9
2	14.0	2.3	4.6	2.3	2.3

a) Initial amount of $Rh(en)_3^{+3}$ in the 6 mL photolysis cell (measured gravimetrically and confirmed spectrophotometrically).

b) Amount of photolysis product, cis-$Rh(en)_2(enH)Cl^{+3}$, at the end of the experiment (measured spectrophotometrically).

c) Initial acid (pH measurement).

d) Final acid (pH measurement).

e) Acid consumed during photolysis ($H^+_{initial}-H^+_{final}$).

to occur before rearrangement of the five-coordinate intermediate can take place. Also, the five-coordinate intermediate is very similar to the $Rh(en)_2(NH_3)^{+3}$ square pyramidal excited state, sp*, in Figure 13. The high energy barrier for rearrangement prevents facile attainment of the TBP* state and therefore, anation occurs in a 100% stereoretentive process.

The choice of chloride as a trapping agent for the coordination site vacated by the formation of a monodentate ethylenediaminum ligand arose from the following factors:

1) If the photolysis product, cis-$Rh(en)_2(enH)Cl^{+3}$, behaves similarly photochemically to $Rh(NH_3)_5Cl^{+2}$,[29] secondary photolysis in 1M Cl^- solution should involve only chloro ligand exchange.

2) In the edge displacement mechanism previously proposed,[14, 28] a chloro ligand is displaced by the free end of the monodentate ethylenediamine ligand. The stability of $Rh(en)_2(enH)Cl^{+3}$ as the photoproduct indicates that the edge displacement mechanism is not operative in the LF photosubstitution reactions of Rh(III) bis(ethylenediamine) mixed ligand complexes.

The photolysis reactions of $Rh(en)_3^{+3}$ in chloride media display isosbestic points throughout the acid concentration range, pH = 0-10. There is a red shift in the isosbestic points at 265 and 244 nm, however, for photolysis at pH = 10. Although the reaction was not further investigated, this shift in isosbestic points is interpreted as the result of the acid-base equilibrium for the protonated-deprotonated form of the monodentate ethylenediamine. Calculations from photolysis spectra place the pK_a of the monocoordinated amine at 9 ± 1.

$$\underline{cis}[Rh(en)_2(enH)Cl]^{+3} \xrightleftharpoons{K_a \simeq 10^{-9}} \underline{cis}\text{-}[Rh(en)_2(mono\text{-}en)Cl]^{+2} + H^+$$

Proton-decoupled C-13 Magnetic Resonance

The proton-decoupled carbon-13 magnetic resonance spectra for all complexes in this study are illustrated in Fgiures 9a-9l with the actual chemical shift values and assignments summarized in Table 5 and Figure 8. The compounds in Figures 9a and 9f-9l are drawn in the Λ configuration, but, in reality, a racemic mixture of Λ and Δ forms are present. Since mirror-image isomers (e.g., Λ-δδδ and Δλλλ) yield identical carbon-13 spectra, the ensuing discussion of the Λ forms of the $Rh(en)_3^{+3}$ and the $\underline{cis}$-$[Rh(en)_2XY]^{+n}$ complexes will be sufficient for all configurational isomers.

Figure 9a displays the C-13 nmr spectrum of the $Rh(en)_3^{+3}$ cation with a single peak at 46.36 ppm (vs. TMS). From proton magnetic resonance, Sudmeier and Blackmer[40] have proposed that the equilibrium popuation of Λ-$[Rh(en)_3]^{+3}$ at 25°C is ∼92% δδλ and ∼8% δδδ. In terms of individual chelate rings, these data correspond to ∼70% δ rings and ∼30% λ rings. The lack of multiple peaks indicates that ring conformational changes are rapid on the nmr time scale. These interpretations are consistent with those of Sudmeier and Blackmer,[40] who have calculated a small free energy difference of ∼1.4 kcal/mol between the Λ-δδλ and Λ-δδδ configurations.

The $\underline{trans}$ complexes (Figures 9b-9c), $\underline{trans}$-$[Rh(en)_2ClX]^{+n}$ (where X = Cl^-, OH_2 and NH_3) and $\underline{trans}$-$[Rh(en)_2(NH_3)(OH_2)]^{+3}$ each display only one carbon-13 resonance occurring at 45.68, 45.75, and 45.64 ppm, respectively, for X = Cl^-, OH_2 and NH_3, and at

45.69 ppm for the trans-$[Rh(en)_2(NH_3)(OH_2)]^{+3}$ species. The presence of only one absorption line is once again, indicative of a rapid $\delta \rightleftharpoons \lambda$ rate of interconversion on the nmr time scale. There are two possible configurations for the two ethylenediamine ligands in the trans-$[Rh(en)_2XY]^{+n}$ species. The two bidentate ethylenediamine ligands can either have the same chirality ($\lambda\lambda$ or $\delta\delta$) or have a different chirality ($\lambda\delta$ or $\delta\lambda$). Corey and Bailar[41] calculated the $\lambda\lambda$ and $\delta\delta$ configurations to be ~1.0 kcal/mol lower in energy than the $\lambda\delta$ configuration. The structural preference results from the position of the amine protons which are eclipsed in the $\lambda\delta$ and staggered in the $\lambda\lambda$ and $\delta\delta$ forms. With these data, a rough calculation can be made on the chemical shift differences that would be required to observe carbon-13 resonances for both configurations at 25°C. Assuming approximately equal populations for the two types of configurations (actually ~85% would be $\lambda\lambda$ and $\delta\delta$ and only ~15% $\lambda\delta$[42]), the minimum frequency difference required for two signals to be resolvable is given by the following equation.[43]

$$2\pi\ \tau\ (\nu_A - \nu_B) = 2 \qquad (31)$$

Using the Arrhenius equation and a 1.0 kcal/mol energy difference between structures[41] to calculate τ, the minimum frequency difference necessary to resolve two signals is $\sim 5 \times 10^{11}$ Hz or 2×10^{10} ppm. Thus it is not surprising that only one carbon-13 is observed for the trans-$[Rh(en)_2XY)]^{+n}$ complexes.

The single carbon-13 resonance signal observed for each *trans*-$[Rh(en)_2XY]^{+n}$ complex ion is relatively insensitive to the nature of X and Y. The values of 45.68, 45.75 and 45.64 ppm, respectively, for X = Cl^-, OH_2 and NH_3 (Y = Cl^-) and 45.69 ppm for X = OH_2 (Y = NH_3), reflect differences that are larger than the spectral reproducibility of $\pm$ 0.03 ppm, but all fall within 0.11 ppm of each other. The perturbation (from electronic changes in the Rh-X bond (or Rh-Y bond) and changes in the remote anisotropic screening due to X(or Y)) due to the change in X (orY) group *cis* to the ethylenediamine ligand must either be small for both effects, or be cancelling influences on the carbon-13 shifts.
This insensitivity to changes in the nature of groups bound *cis* to ethylenediamine ligands is also observed in the carbon-13 magnetic resonance of *trans*-$[Co(en)_2XY]^{+n}$ complex ions,[44] where the single carbon resonances appear at 46.0 ppm (X = Y = Cl^-), 45.7 ppm (X = Y = NO_2), 46.0 ppm (X = Y = NCS^-), and 46.0 ppm (X = Cl^-, Y = NCS^-).

The carbon-13 nmr spectra of the *cis* complexes, *cis*-$[Rh(en)_2XY]^{+n}$ (where X = Cl^-, OH_2, NH_3 and enH^+ (NH_2-CH_2-CH_2-NH_3^+) and Y = Cl^-, NH_3), are illustrated in Figures 9f-91. Once again, no multiple peaks which could be assigned to λ and δ ring conformational differences are observed. The calculation of a minimum chemical shift difference necessary to observe peak separation is more complicated for the *cis* isomers than the *trans* isomers. The most symmetrical *cis* complex, *cis*-$[Rh(en)_2Cl_2]^+$, can exist in three chemically non-equivalent forms. Using the Λ isomer as a model,

the ethylenediamine ligands can exist in the λλ, λδ or δδ conformations, which have 2, 4 and 2 non-equivalent carbon atoms, respectively. Thus, unlike the trans isomers, where two forms are in equilibrium, the cis isomer has three forms (λλ,λδ and δδ) conformations) spanning an energy range on the order of 1-3 kcal/mol, and the nmr experiment will only produce the average configurational resonance signal.

Figures 9f and 9g display the carbon-13 nmr signal of cis-$[Rh(en)_2Cl_2]NO_3$ and cis-$[Rh(en)_2Cl_2]ClO_4$, respectively. Figure 9f is virtually identical to the spectrum previously reported for this complex.[45] The three signals, first reported[45] as being the result of slow $\lambda \rightleftharpoons \delta$ interconversions on the nmr time scale, are unequivocally due to a mixture of cis- and trans-$[Rh(en)_2Cl_2]^+$. A rough calculation of the relative intensities of the signals in Figure 9f indicate that the trans impurity makes up about 20% of the sample. This composition is consistent with previously discussed calculations from the electronic spectra.

Figures 9h, 9i and 9l illustrate the proton-decoupled carbon-13 spectra of cis-$[Rh(en)_2(OH_2)Cl]^{+2}$, cis-$[Rh(en)_2(OH_2)(NH_3)]^{+3}$ and cis-$[Rh(en)_2(NH_3)Cl]^{+2}$ complex ions. Each spectrum displays signals assignable to four carbon atoms. The spectrum of cis-$Rh(en)_2(NH_3)Cl^{+2}$ displays only three resonance signals, but the peak at 45.81 ppm is approximately double the intensity of the other two peaks and no doubt reflects a coincidence (within experimental limits) of two carbon resonances. The broadening or slight

splitting of the resonances of these compounds is possibly due to coupling of the carbon-13 nuclei to rhodium-103 (S = 1/2, 100% abundance). One can discount λ and δ conformational changes as the reason for peak splitting, since resolution of conformations with such similar chemical shifts would require a large free energy difference between conformations.[43] Any free energy difference larger than 1 kcal/mol would lead to an equilibrium mixture containing $\geq$ 85% of the more stable conformer.[42] Since the split peaks are approximately the same intensity, splitting *via* spin-spin coupling is a more reasonable assumption.

A comparison of the chemical shifts of the series of *cis*-$[Rh(en)_2XY]^{+n}$ complexes (where X = Cl^-, OH_2, NH_3, Y = Cl^-, NH_3) indicates that large chemical shift differences are observed when X (or Y) is varied. The similar comparison for *trans*-$[Rh(en)_2XY]^{+n}$ complexes (X and Y are always *cis* to the ethylenediamines) indicates that the carbon-13 chemical shifts are insensitive to X and Y. The relatively small "cis effect" and relatively large "trans effect" can arise from effects such as neighboring group anisotropy and electronic effects. The change in chemical shift as a function of neighboring group anisotropy is given by equation 32:

$$\Delta\sigma = \frac{1-3\cos^2\theta}{3R^3}\,(\chi_{\parallel}-\chi_{\perp}) \qquad (32)$$

where θ is the angle between interacting nuclei and R is the through-space distance. For the *trans* complexes, the value of θ between

all four carbon atoms and X and Y lies between 40° and 60° and $\Delta\sigma$ is small. The cis complexes have a variety of Θ values between the carbon atoms and X and Y, some of which lead to relatively large values of $1-3\cos^2\Theta$. Thus, neighboring group anisotropy due to X and Y can be very sensitive to the nature of the unidentate ligands (i.e., χ_{11} and χ of X and Y), while changes in X and Y do not substantially alter σ in the trans complexes due to the presence of a small geometric factor in equation 32.

A corresponding result is obtained when electronic effects are considered. Changing the unique ligand X(Y) should cause the greatest changes in electronic distribution at the ligand trans rather than cis to X(Y).[5] In the trans complexes, X and Y are trans to each other, while an ethylenediamine nitrogen always occupies the sites trans to X and Y in the cis complexes. Therefore, greater changes are expected in electronic distribution around carbon atoms in the cis complexes, and greater chemical shift differences are observed in their carbon-13 nmr spectra.

Based on the carbon-13 nmr spectrum of a photolyzed sample of $Rh(en)_3^{+3}$ (Figures 9j and 9k), a cis configuration has been assigned to the photoproduct, $[Rh(en)_2(enH)Cl]^{+3}$. In addition to the four resonances observed in the chemical shift region, typical of the other cis-$[Rh(en)_2XY]^{+n}$ complexes, two additional upfield resonances are displayed at 43.30 ppm and 40.59 ppm, and these resonances can be assigned to the carbon atoms in the ethylenediaminum ligand; the carbon atom α to the quarternary nitrogen atom is assigned to the 40.59 ppm signal. This resonance is deshielded with respect

to the other signals due to polarization of the α-carbon-nitrogen bond as a result of nitrogen protonation.[46] The broadening of this signal is also typical of carbon atoms which are α to quarternary nitrogens.[47] The carbon-13 nmr spectrum of the photolysis mixture is shown in Figure 9j. The presence of unreacted starting material ($[Rh(en)_3]^{+3}$) and secondary photolysis product (trans-$[Rh(en)_2Cl_2]^+$) has been confirmed by spiking the sample with the impurities. Computer subtraction techniques, using authentic spectra of $[Rh(en)_3]^{+3}$ and trans-$[Rh(en)_2Cl_2]^+$, result in the spectrum shown in Figure 9k, which corresponds to a spectrum of pure cis-$[Rh(en)_2(enH)Cl]^{+3}$.

Tentative assignments of chemical shifts to the particular non-equivalent carbon atoms are based on the relatively large "trans effect" (Figure 8 and Table 5). While the similarity of chemical shifts for the trans-$[Rh(en)_2XY]^{+n}$ (seemingly independent of either X or Y) is indicative of the effect of trans nitrogen ligands, other shift effects of unknown origin are manifested in these complexes, as demonstrated by the downfield shift in the spectrum of $[Rh(en)_3]^{+3}$.

The carbon-13 nmr spectrum of cis-$[Rh(en)_2Cl_2]^+$ displays two signals at 46.15 and 47.25 ppm. The former shift is assigned to two carbons, α to nitrogens trans to each other (a and a'), whereas the latter shift is assigned to the two carbon atoms trans to the chloro ligands (b and b'). These assignments are consistent with the large "trans effect", whereby the electronegative trans chloro ligands more effectively deshield the proximal carbon atoms (a and a') than the distal carbon atoms (b and b').

A similar approach was used in the assignment of carbon atom resonances for cis-$[Rh(en)_2ClY]^{+n}$ where Y = OH_2, NH_3, and enH^+. The small "cis effect" observed for the trans-$[Rh(en)_2ClY]^{+n}$ complexes, suggests that the a' and b' carbon atoms should be relatively insensitive to various Y ligands. This observation leads to the assignments of 46.15, 45.98, 45.81 and 45.94 ppm for the a' carbon atoms, and 47.25, 47.07, 47.07 and 47.15 ppm for the b' carbon atoms in cis-$[Rh(en)_2ClY]^{+n}$, where Y + Cl^-, OH_2, NH_3 and enH^+, respectively. The largest differences in the series should be observed for the b carbon atom which is directly bound to the nitrogen atom trans to the changing Y ligand. Resonances have been tentatively assigned at 47.25, 47.78, 45.81 and 45.99 ppm for the b carbon atom when Y = Cl^-, OH_2, NH_3 and enH^+, respectively. The assignments for the a carbon atoms are then 46.15, 45.20, 46.27 and 46.56 ppm, respectively, for Y = Cl^-, OH_2, NH_3 and enH^+. The cis-$[Rh(en)_2(NH_3)Cl]^{+2}$ and cis-$[Rh(en)_2(enH)Cl]^{+3}$ have their a carbon atoms in an environment that is electronically and magnetically similar to the carbon atoms in $[Rh(en)_3]^{+3}$. Our assignments place these a carbon atoms at 46.27 and 46.56 ppm, respectively, in agreement with this observation.

The carbon atom assignments for cis-$[Rh(en)_2(OH_2)(NH_3)]^{+3}$ are deduced from the assignments for cis-$[Rh(en)_2Cl(OH_2)]^{+2}$ and cis-$[Rh(en)_2Cl(NH_3)]^{+2}$. Carbon atoms a and b are "trans" to NH_3 in both the cis-$[Rh(en)_2(OH_2)(NH_3)]^{+3}$ and cis-$[Rh(en)_2Cl(NH_3)]^{+2}$ complexes, and carbon atoms a and b in the former compound are assigned to the 46.39 and 45.99 ppm resonances, respectively.

Carbon atoms a' and b' for the cis-$[Rh(en)_2(OH_2)(NH_3)]^{+3}$ species, are assigned the 45.03 and 47.68 ppm resonance, respectively, in agreement with the previously stated conclusion of a dominant "trans effect".

Although these tentative assignments appear to be internally consistent, the limited knowledge concerning neighboring group anisotropic effects, electronic effects, and solvent effects, prevents the unequivocal assignment of the carbon-13 resonances.

REFERENCES

REFERENCES

1. J. F. Endicott, ch. 3, p. 124, "Concepts of Inorganic Photochemistry", A.W. Adamson, P.D. Fleischauer, editors, Wiley-Interscience, 1975.

2. G. Stein, Israel J. Chem., 8, 691 (1970).

3. A.F. Vaudo, E.R. Kantrowitz and M.F. Hoffman, J. Amer. Chem. Soc., 93, 6698 (1971).

4. (*) super notation refers to antibonding molecular orbitals.

5. K.F. Purcell and J.C. Kotz, "Inorganic Chemistry", W.B. Saunders Co., Philadelphia, Pa., 1977.

6. H.F. Wasgestian and H.L. Schlafer, Z. Phys. Chem. (Frankfurt am Main), 57, 282 (1968).

7. E. Zinato, R.D. Lindholm, and A.W. Adamson, J. Amer. Chem. Soc., 91, 1076 (1969).

8. P. Riccieri and H.L. Schlafer, Inorg. Chem. 9, 727 (1970).

9. C.S. Garner and D.A. House, Transition Metal Chem., 6, 59 (1970).

10. E. Zinato, R. Riccieri, and A.W. Adamson, J. Amer. Chem. Soc., 96, 375 (1974).

11. (a) M.T. Gandolfi, M.F. Manfrin, A. Juris, L. Moggi, and V. Balzani, Inorg. Chem., 13, 1342 (1974). (b) C.F.C. Wong and A.D. Kink, Inorg. Chem., 15, 1519 (1976).

12. A.W. Adamson, J. Phys. Chem., 71, 798 (1967).

13. (a) M. Wrighton, H.B. Gray, and G.S. Hammond, Mol. Photochem., 5, 165 (1973); (b) J.I. Fink, J. Amer. Chem. Soc., 94, 8039 (1972).

14. (a) R.A. Pribush, C.K. Poon, C.M. Bruce, and A.W. Adamson, J. Amer. Chem. Soc., 96, 3027 (1974; (b) P.S. Sheridan and A.W. Adamson, J. Amer. Chem. Soc., 96, 3032 (1974).

15. M.D. Alexander and C.A. Spillert, Inorg. Chem., 9, 2344 (1970).

16. A.W. Adamson, Advances in Chemistry Series, R. Bruce King, ed., 150, 128 (1976).

17. P.S. Sheridan and A.W. Adamson, Inorg. Chem., 13, 2482 (1974).

18. J.K. Burdett, Inorg. Chem., 15, 212 (1976).

19. P.S. Sheridan, unpublished observation.

20. C.H. Langford and C.P.J. Vuik, J. Amer. Chem. Soc., 98, 5409 (1976).

21. J.F. Endicott and G.J. Ferraudi, J. Phys. Chem., 80 949 (1976).

22. T.L. Kelly and J.F. Endicott, J. Phys. Chem., 76, 1937 (1972).

23. J.D. Petersen and P.C. Ford, J. Phys. Chem., 78, 1144 (1974).

24. M.K. De Armond and J.E. Hillis, J. Chem. Phys., 54, 2247 (1971).

25. T.L. Kelly and J.F. Endicott, J. Amer. Chem. Soc., 94, 278 (1972).

26. T.R. Thomas, R.J. Watts, and G.A. Crosby, J. Chem. Phys., 59, 2923 (1973).

27. D. Strauss and P.C. Ford, J.C.S. Chem. Comm. 1977, 194.

28. M.M. Muir and W. Huang, Inorg. Chem., 12, 1831 (1973).

29. P.C. Ford and J.D. Petersen, Inorg. Chem., 14, 1404 (1975).

30. F. Galsbøl, Inorg. Synth., 12, 269 (1970).

31. S.A. Johnson and F. Basolo, Inorg. Chem., 1, 925 (1962).

32. P. Sheridan, private communication.

33. C. Burgess, F.R. Hartley, and D.E. Rogers, Inorg. Chim. ACTA, 13, 35 (1975).

34. G.G. Hatchard and C.A. Parker, Proc. Roy Soc., Ser. A, 235, 518 (1956).

35. Isomerization may in fact occur sooner, but three weeks is the actual time interval between the synthesis and the photolysis experiments.

36. C. Kutal and A.W. Adamson, Inorg. Chem., 12, 1454 (1973).

37. C.E. Schaeffer, Structure and Bonding, 5, 68 (1968).

38. J.I. Zink, Inorg. Chem., 12, 1018 (1973).

39. F. Monacelli, Inorg. Chim. ACTA, 2, 263 (1968).

40. J.L. Sudmeier, G.L. Blackmer, Inorg. Chem., 10, 2010 (1971).

41. E.J. Corey, J.C. Bailar, Jr., J. Amer. Chem. Soc., 81, 2620 (1959).

42. E.L. Eltel, "Stereochemistry of Carbon Compounds", McGraw-Hill Series In Advanced Chemistry, McGraw-Hill, New York, 1962, inside back cover.

43. J.A. Pople, W.G. Schneider, and H.F. Bernstein, "High Resolution Nuclear Magnetic Resonance", McGraw-Hill Series In Advanced Chemistry, McGraw-Hill, New York, 1959, p. 223.

44. D.A. House and J.W. Blunt, Inorg. Nucl. Chem. Lett., 11, 219 (1975).

45. C. Burgess and F.R. Hartley, Inorg. Chim. ACTA, 14, 37 (1975).

46. R.J. Pugmire and D.M. Grant, J. Amer. Chem. Soc., 90, 697 (1968). J.E. Figard, J.V. Paukstelis, E.F. Byrne, and J.D. Petersen, J. Amer. Chem. Soc., 99, 8417 (1977).

47. N.J.M. Birdsall, J. Feeney, A.G. Lee, Y.K. Levine, and J.C. Metcalfe, J. Chem. Soc., Perkin II, 1441 (1972). H.H. Mantsch and I.C.P. Smith, Canad. J. Chem., 51, 1384 (1973). M. Hansen and H.J. Jakobson, ACTA Chem. Scand., 26, 2548 (1972).

48. E.E. Wegner and A.W. Adamson, J. Amer. Chem. Soc., 88, 394 (1966).

49. F. Basolo and R. Pearson, "Mechanisms of Inorganic Reactions; A Study of Metal Complexes in Solution", J. Wiley & Sons, Inc., 2nd ed., 1967, pp. 164, 168, 171.

50. W. Geis and H.L. Schlafer, Z. Phys. Chem. (Frankfurt), 65, 107 (1969).

51. P. Riccieri and E. Zinato, Proceedings of the XIV Internat'l Conference On Coordination Chemistry, IUPAC, Toronto, Canada, 1972, p. 252.

52. A.D. Kirk, K.C. Moss, and J.G. Valentin, Canad. J. Chem., 49, 1524 (1971).

53. H.F. Wasgestian and H.L. Schlafer, Z. Phys. Chem. (Frankfurt), 62, 127 (1968).

54. M.F. Manfrin, G. Varani, L. Moggi, and V. Balzani, Molec. Photochem., 1, 387 (1969).

APPENDICES

APPENDIX 1. Computer Program and Instructions for Quantum Yield Calculation.

INSTRUCTIONS

1) Clear, GO TO 0000, LOAD
2) Feed magnetic card through reader.
3) GO TO 0000, CONTINUE
4) Enter "v", ↑, "l", ↑ "Δε", CONTINUE
5) Enter I_o^i, ↑, total absorbance change, CONTINUE
6) Enter A^i_{mon}, ↑, A^i_{irr}, ↑, A^i_{irr}, CONTINUE
7) Enter t, ↑, A^t_{mon}, ↑, A^t_{irr}, CONTINUE
8) Repeat Step 7) until all data points have been entered, then SET FLAG, CONTINUE

OUTPUT (for each t)

Φ overall

% reaction

Φ incremental

INPUT

"v" - volume of cell (ml)

"l" - pathlength of cell (cm)

"Δε" - difference in molar absorptivity coefficients between reactant and product at monitored wavelength ($M^{-1}cm^{-1}$)

I_o^i - Output of lamp (quanta/min)

total absorbance change - change at monitored wavelength if reaction goes to 100%

A^i_{mon} - chart reading at monitored wavelength (t=0)

A^i_{irr} - chart reading at irradiating wavelength (t=0)

$|A^i_{irr}|$ - actual absorbance at irradiating wavelength (t=0)

t - time (min)

A^t_{mon} - chart reading at monitored wavelength (time t)

A^t_{irr} - chart reading at irradiating wavelength (time t)

APPENDIX 1 (cont'd). Computer Program for Calculating Quantum Yields.

(Hewlett-Packard 9810 A Calculator)

STEP#	CODE	STEP#	CODE	STEP#	CODE	STEP#	CODE	STEP#	CODE	STEP#	CODE
0000	20	0051	23	0101	27	0151	00	0201	67	0251	25
0001	41	0052	00	0102	15	0152	74	0202	00	0252	45
0002	36	0053	00	0103	40	0153	32	0203	01	0253	45
0003	25	0054	11	0104	00	0154	27	0204	04	0254	44
0004	35	0055	40	0105	01	0155	01	0205	36	0255	00
0005	40	0056	00	0106	03	0156	33	0206	06	0256	00
0006	00	0057	01	0107	67	0157	24	0207	21	0257	04
0007	00	0058	00	0108	00	0158	36	0208	00	0258	04
0008	00	0059	67	0109	01	0159	00	0209	02	0259	45
0009	41	0060	34	0110	00	0160	00	0210	03	0260	45
0010	40	0061	00	0111	23	0161	01	0211	26	0261	45
0011	00	0062	00	0112	00	0162	24	0212	02	0262	45
0012	00	0063	06	0113	00	0163	36	0213	00	0263	45
0013	01	0064	24	0114	10	0164	14	0214	36	0264	45
0014	23	0065	34	0115	67	0165	40	0215	25	0265	45
0015	00	0066	00	0116	34	0166	00	0216	45	0266	45
0016	00	0067	00	0117	00	0167	01	0217	67	0267	45
0017	02	0068	10	0118	00	0168	05	0218	00	0268	46
0018	41	0069	15	0119	07	0169	67	0219	01		
0019	23	0070	40	0120	27	0170	01	0220	04		
0020	00	0071	00	0121	15	0171	03	0221	67		
0021	00	0072	01	0122	40	0172	27	0222	35		
0022	03	0073	01	0123	00	0173	02	0223	00		
0023	23	0074	22	0124	01	0174	35	0224	00		
0024	00	0075	15	0125	04	0175	24	0225	02		
0025	00	0076	40	0126	67	0176	34	0226	45		
0026	04	0077	00	0127	00	0177	00	0227	67		
0027	40	0078	01	0128	00	0178	00	0228	00		
0028	00	0079	02	0129	04	0179	03	0229	00		
0029	00	0080	27	0130	27	0180	01	0230	00		
0030	05	0081	67	0131	67	0181	00	0231	67		
0031	40	0082	34	0132	00	0182	74	0232	36		
0032	00	0083	13	0133	01	0183	32	0233	00		
0033	00	0084	23	0134	02	0184	27	0234	01		
0034	06	0085	14	0135	34	0185	01	0235	01		
0035	25	0086	40	0136	27	0186	33	0236	67		
0036	40	0087	13	0137	02	0187	24	0237	35		
0037	00	0088	67	0138	35	0188	36	0238	00		
0038	00	0089	00	0139	24	0189	00	0239	01		
0039	07	0090	00	0140	34	0190	00	0240	05		
0040	40	0091	11	0141	00	0191	01	0241	27		
0041	00	0092	23	0142	00	0192	24	0242	06		
0042	00	0093	00	0143	04	0193	36	0243	21		
0043	10	0094	00	0144	25	0194	13	0244	00		
0044	41	0095	06	0145	40	0195	67	0245	02		
0045	57	0096	67	0146	00	0196	00	0246	03		
0046	43	0097	34	0147	00	0197	00	0247	26		
0047	00	0098	00	0148	04	0198	00	0248	02		
0048	02	0099	00	0149	27	0199	30	0249	00		
0049	05	0100	05	0150	01	0200	35	0250	36		
0050	11										

APPENDIX 2

Lf Photochemical Data for Rh(III) Amine Complexes. All photolyses @ 25 C except where noted.

Compound	Conditions	$I_o^i(10^{17}q/min)$	overall	% rxn	Reference
$Rh(en)_3^{+3}$	15 C, 1 M Cl^-, pH=0,313 nm	11.5	0.034	27.7	14-1-1
	15 C	9.64	0.030	14.6	22'-1-1(JDP) [a,b]
	15 C	9.64	0.028	14.0	22'-1-2(JDP)
	20 C	9.05	0.032	19.5	15-1-1
	20 C	9.05	0.031	18.3	15-1-2
	20 C	6.9	0.047	13.7	15'-1-1
	20 C	6.9	0.049	12.8	15'-1-2
	25 C, 1 M Cl^-, pH=0,313 nm	4.2	0.039	10.7	17'-1-1
		4.2	0.028	9.0	17'-1-2
		10.9	0.046	20.8	21-1-1
		9.3	0.039	17.5	21-1-2
	20 C, 1 M Cl^-, pH=2,313 nm	4.7	0.050	11.9	16'-1-1
		4.7	---	10.1	16'-1-2
		3.7	0.049	9.7	18-1-1
		3.7	0.048	10.8	18-1-2
		8.9	---	21.3	21'-1-1
		8.4	0.035	16.3	22-1-1
		7.7	0.034	15.7	22-1-2
	20 C, 1 M Cl^-, pH=4,313 nm	4.5	0.043	10.8	17-1-1
	25 C, 1 M Cl^-, pH=4,313 nm	14.1	0.045	24.3	20'-1-1
		11.2	0.048	22.5	20'-1-2
	25 C, 1 M Cl^-, pH=6,313 nm	7.4	0.037	16.1	22'-1-1
		6.3	0.037	16.7	22'-1-2
	25 C, 1 M Cl^-, pH=8,313 nm	4.9	0.037	11.6	23-1-1
		4.3	---	9.8	23-1-2
	25 C, 1 M Cl^-, pH=10,313 nm	4.3	0.039	17.2	24'-1-1
		3.5	0.040	17.0	24'-1-2
	25 C, 1 M Cl^-, pH=12,313 nm	3.5	---	13.6	25-1-1
		3.1	---	12.4	25-1-2

APPENDIX 2 (continued)

Compound	Conditions	$I_o^i(10^{17}$ q/min)	overall	% rxn	Reference
$Rh(en)_3^{+3}$	25 C, 0.5 M Cl^-, pH=2,313 nm	2.45	0.036	11.8	26-1-1
	25 C, 2 M Cl^-, pH=2,313 nm	3.98	0.031	8.3	27'-1-1
		3.4	---	8.1	27'-1-2
		2.2	0.041	4.85	28-1-1
		2.2	0.040	7.0	28-1-2
		2.8	0.036	7.5	29-1-1
		2.7	0.042	7.2	29-1-2
c-$Rh(en)_2Cl_2^+$	25 C, 0.014 N $HClO_4$, 365 nm	25.2	0.44	50.0	31'-1-2
		25.2	0.45	44.1	31'-1-3
		25.2	0.41	45.8	33-1-1
		25.2	0.44	39.0	33-1-2
t-$Rh(en)_2Cl_2^+$	25 C, 0.014 N $HClO_4$, 405 nm	33.2	0.063	50.0	32-1-2
		24.5	0.065	21.4	34-1-1
		24.5	0.069	25.0	34-1-2
		27.3	0.060	24.3	34'-1-1
		27.3	0.059	25.0	34'-1-2
c-$Rh(en)_2(NH_3)Cl^{+2}$	25 C, 0.014 N $HClO_4$, 365 nm	8.8	0.16	37.0	53'-1-1
		8.5	0.14	31.0	53'-1-2
		9.8	0.135	40.8	55-1-1
		9.8	0.146	45.6	55-1-2
t-$Rh(en)_2(NH_3)Cl^{+2}$	25 C, 0.014 N $HClO_4$, 365 nm	12.2	0.067	12.6	49-1-1
		12.2	0.063	12.9	49-1-2
		11.4	0.050	9.7	48'-1-1
		12.9	0.078	14.2	44-1-2
		12.9	0.062	15.8	44-1-1

a) Primed numbers refer to yellow pages in laboratory notebook. b) Experiment run by J.D.Petersen.

APPENDIX 3 : The Angular Overlap Model (AOM)

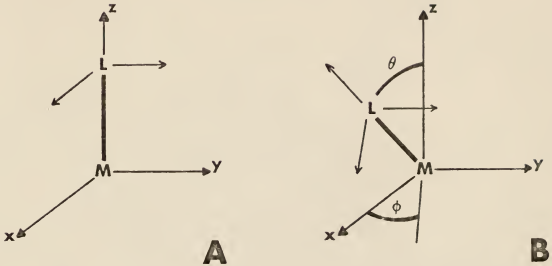

A. Diatomic molecule with coordinate system drawn in such a way that the overlap integrals $S_\sigma = \langle d_{z^2} | \sigma_L \rangle$, $S_{\pi x} = \langle d_{xz} | p_x \rangle$ and $S_{\pi y} = \langle d_{yz} | p_y \rangle$ are maximum for the M-L distance. This is the same as saying that the basis orbitals are diagonals

B. This illustrates how any position on a sphere around the metal ion M can be reached from the position on the positive z-axis by rotation around the y-axis an angle θ ($0 < \theta \leq 180°$) and an angle ϕ ($0 \leq \phi < 360°$) around the z-axis. By rotating an angle ψ around z_L (z-axis of ligand, L), the x_L and y_L coordinates can be brought parallel to a chosen coordinate system on the sphere.

APPENDIX 3 (cont'd)

DIAGONAL MATRIX ELEMENTS: $\langle d_i | V_{LF} | d_i \rangle = \sum_{\lambda\omega} \sum_{n=1}^{N} e_{\lambda n} \cdot F(d_i, L_n)^2$

OFF-DIAGONAL MATRIX ELEMENTS: $\langle d_i | V_{LF} | d_j \rangle = \sum_{\lambda\omega} \sum_{n}^{N} e_{\lambda n} \cdot F_{\lambda\omega}(d_i, L_n) \cdot F_{\lambda\omega}(d_j, L_n)$

Where λ stands for σ or π interactions, ω specifies the two (x and y) π interactions, F is the fraction of maximum overlap integral.

	$F_\sigma(d, L(\Theta, \phi, \psi))$	$F_{\pi y}(d, L(\Theta, \phi, \psi))$	$F_{\pi x}(d, L(\Theta, \phi, \psi))$
dz^2	$(1 + 3 \cos 2\Theta)/4$	$\sqrt{\frac{3}{2}} \sin 2\Theta \sin \psi$	$-\sqrt{\frac{3}{2}} \sin 2\Theta \cos \psi$
dyz	$\sqrt{\frac{3}{2}} \sin \phi \sin 2\Theta$	$(\cos \psi \cos \Theta \cos \psi$ $-\sin \psi \cos 2\Theta \sin \psi)$	$(\cos \phi \cos \Theta \sin \psi$ $+ \sin \phi \cos 2\Theta \cos \psi)$
dxz	$\sqrt{\frac{3}{2}} \cos \phi \sin 2\Theta$	$(-\sin \phi \cos \Theta \cos \psi$ $-\cos \phi \cos 2\Theta \sin \psi)$	$(-\sin \phi \cos \Theta \sin \psi$ $+ \cos \phi \cos 2\Theta \cos \psi)$
dxy	$\sqrt{\frac{3}{4}} \sin 2\Theta(1-\cos 2\Theta)$	$(\cos 2\phi \sin \Theta \cos \psi$ $-1/2 \sin 2\phi \sin 2\Theta \sin \psi)$	$(\cos 2\phi \sin \Theta \sin \psi$ $+ 1/2 \sin 2\phi \sin 2\Theta \cos \psi)$
$d_{x^2-y^2}$	$\sqrt{\frac{3}{4}} \cos 2\phi (1-\cos 2\Theta)$	$(-\sin 2\phi \sin \Theta \cos \psi$ $-1/2 \cos 2\phi \sin 2\Theta \sin \psi)$	$(-\sin 2\phi \sin \Theta \sin \psi$ $+ 1/2 \cos 2\phi \sin 2\Theta \cos \psi)$

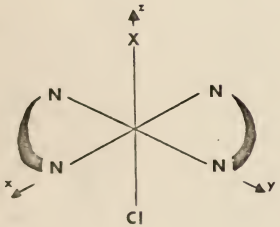

	z^2	x^2-y^2	yz	xz	xy
z^2	$1e_\sigma^X + 1e_\sigma^{Cl} + 1e_\sigma^N$	0	0	0	0
x^2-y^2		$3e_\sigma^N$	0	0	0
yz			$1e_\pi^{yX} + 1e_\pi^{yCl}$	0	0
xz				$1e_\pi^{xX} + 1e_\pi^{xCl}$	0
xy					0

GSSE: $2e_\sigma^X + 2e_\sigma^{Cl} + 8e_\sigma^N$

ESSE: $1e_\pi^X + 1e_\pi^{Cl} + 1e_\sigma^X + 1e_\sigma^{Cl} + 7e_\sigma^N$

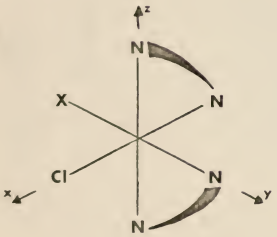

	z^2	x^2-y^2	yz	xz	xy
z^2	$.25e_\sigma^X + .25e_\sigma^{Cl} + 2.5e_\sigma^N$	0	0	0	0
x^2-y^2		$.75e_\sigma^X + .75e_\sigma^{Cl} + 1.5e_\sigma^N$	0	0	0
yz			$1e_\pi^{xX}$	0	0
xz				$1e_\pi^{xCl}$	0
xy					$1e_\pi^{yX} + 1e_\pi^{yCl}$

GSSE: $2e_\sigma^X + 2e_\sigma^{Cl} + 8e_\sigma^N$

ESSE: $1e_\pi^X + 1e_\pi^{Cl} + 1.25e_\sigma^X + 1.25e_\sigma^{Cl} + 6.5e_\sigma^N$

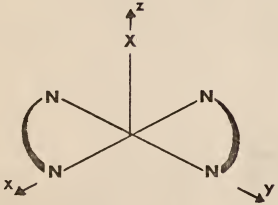

GSSE: $2e_{\sigma}^{X} + 8e_{\sigma}^{N}$

ESSE: $1e_{\pi}^{X} + 1e_{\sigma}^{X} + 7e_{\sigma}^{N}$

	z^2	x^2-y^2	yz	xz	xy
z^2	$1e_{\sigma}^{X} + 1e_{\sigma}^{N}$	0	0	0	0
x^2-y^2		$3e_{\sigma}^{N}$	0	0	0
yz			$1e_{\pi}^{yX}$	0	0
xz				$1e_{\pi}^{xX}$	0
xy					0

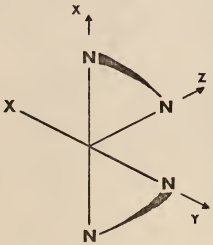

GSSE: $2e_{\sigma}^{X} + 8e_{\sigma}^{N}$

ESSS: $1e_{\pi}^{X} + 1.75e_{\sigma}^{X} + 6.25e_{\sigma}^{N}$

	z^2	x^2-y^2	yz	xz	xy
z^2	$.25e_{\sigma}^{X} + 1.75e_{\sigma}^{N}$	$\sqrt{3}/4e_{\sigma}^{N} - \sqrt{3}/4e_{\sigma}^{X}$	0	0	0
x^2-y^2		$.75e_{\sigma}^{X} + 2.25e_{\sigma}^{N}$	0	0	0
yz			0	0	0
xz				$1e_{\pi}^{X}$	0
xy					$1e_{\pi}^{X}$

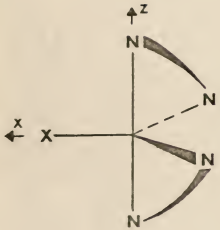

	z^2	x^2-y^2	yz	xz	xy
z^2	$.25e_\sigma^X + 2.5e_\sigma^N$	$\sqrt{3}/4e_\sigma^N - \sqrt{3}/4e_\sigma^X$	0	0	$-.75e_\sigma^N$
x^2-y^2		$.75e_\sigma^X + 3/8e_\sigma^N$	0	0	0
yz			0	0	0
xz				$1e_\pi^X$	0
xy					$1e_\pi^X + 9/8e_\sigma^N$

GSSE: $2e_\sigma^X + 5.75e_\sigma^N$

ESSE: $1e_\pi^X + 1.25e_\sigma^X + 5.75e_\sigma^N$

ABBREVIATIONS

LIGANDS

en	ethylenediamine
trien	triaminotriethylamine

EXCITED STATE GEOMETRIES

sp	square pyramid (X equatorial)
sp'	square pyramid (X axial)

ANGULAR OVERLAP MODEL (AOM)

GSSE	ground state stabilization energy
ESSE	excited state stabilization energy

ABSTRACT

THE PHOTOCHEMISTRY OF RHODIUM(III) AMINE COMPLEXES

by

Frank Peter Jakse

B.S., Illinois Benedictine College, 1975

AN ABSTRACT OF A MASTER'S THESIS

submitted in partial fulfillment of the

requirements for the degree

MASTER OF SCIENCE

Department of Chemistry

KANSAS STATE UNIVERSITY
Manhattan, Kansas

1978

The work reported in this paper deals with the ligand field (LF) reactivity for the general complex, $[Rh(en)_2XY]^{+n}$, where en = ethylenediamine, X = en/2, Cl^-, NH_3, and Y = en/2, Cl^-, OH_2. Utilizing the tools of carbon-13 nmr spectroscopy and UV-vis electronic spectroscopy, the stereochemistry of the photolysis product is determined, and a reaction mechanism is developed that is generally applicable to the LF reactivity of all Rhodium(III) amine mixed-ligand complexes.

For the trans-$[Rh(en)_2ClX]^{+n}$ complexes (X = Cl^-, NH_3, OH_2), LF photolysis produces labilization of chloro ligand, and stereo-retentive aquation of the five-coordinate intermediate, $[Rh(en)_2X]^{+n}$, yields exclusively trans-$[Rh(en)_2(OH_2)X]^{+(n+1)}$. For the corresponding cis complexes, the stereochemical course of the reaction is dependent on the liquid X:X=Cl^-, 100% trans-$[Rh(en)_2(OH_2)Cl]^{+n}$; X = NH_3, predominant cis-$[Rh(en)_2(NH_3)(OH_2)]^{+3}$. LF photolysis of $Rh(en)_3^{+3}$ in aqueous Cl^- and at various pH's yields cis-$[Rh(en)_2(enH)Cl]^{+3}$, where enH is the protonated monodentate ethylenediamium ligand.

Proton-decoupled carbon-13 nmr spectra are presented for all complexes studied in this research. While many spectra were obtained for the complex's isolated salt (dissolved in a H_2O/D_2O (1:1, v/v) solution), some spectra were obtained in situ of the photolyzed solution in order to determine the isomeric composition of the photoproduct.

A mechanistic interpretation is advanced that is consistent with the LF reactivity observed thus far for the family of Rh(III) amines. The stereochemical course of the reaction is

presented *via* a potential energy analysis of the five-coordinate intermediate's geometry in the excited state. The mechanism is not only applicable to the Rhodium(III) complexes studied in this research, but it is also consistent with the reactivity of previously studied Rh(III) amine species.